Practical Consequences of Inertia Shaping for Interaction and Tracking in Robot Control

Alexander Dietrich[a,*], Xuwei Wu[a], Kristin Bussmann[a], Marie Harder[a], Maged Iskandar[a], Johannes Englsberger[a], Christian Ott[a], Alin Albu-Schäffer[a,b]

[a] *Institute of Robotics and Mechatronics, German Aerospace Center (DLR), Münchener Strasse 20, 82234, Wessling, Germany*
[b] *Department of Informatics, Technical University of Munich (TUM), Boltzmannstrasse 3, 85748, Garching, Germany*

Abstract

In trajectory tracking and interaction control of robots, two fundamentally different concepts define the boundaries within which most nonlinear model-based approaches can be located. On the one hand controllers such as the PD+ preserve the natural inertia and avoid feedback of external forces and torques. On the other hand controllers based on feedback linearization, as used in most inverse dynamics approaches, enforce linear closed-loop dynamics by means of external force/torque feedback. Here, these two basic concepts of keeping and shaping of the natural inertia are investigated and compared including aspects such as interaction behavior, tracking performance, tuning parameters, influence of modeling errors, and effective feedback gains. Exemplary case studies on a standard torque-controlled robot are performed. The understanding of these features and differences is of major importance for the proper selection and deployment of interaction and tracking controllers in practice.

Keywords: Robotics, control, inertia shaping, PD+, feedback linearization

1. Introduction

When robots with joint torque interface are used both for trajectory tracking and physical interaction, the so-called *computed-torque controller* [1] is often the means of choice. In fact, it is basically an application of the more general concept of *feedback linearization* [2]. The major advantage is the linear closed-loop dynamics which opens the possibility to use any tools from linear control theory. Moreover, by rendering the system linear one can specify desired impedance characteristics including the inertia, damping, and stiffness parametrization [3]. Yet it is well known that compensating for all naturally nonlinear dynamic effects requires both highly precise measurements and accurate model knowledge. That, in turn, can come at the cost of deteriorated performance in practice or even instability if these requirements are not sufficiently met.

An alternative way is to reduce the feedback action to a minimum by conserving the natural, nonlinear dynamics as much as possible and still achieve proper trajectory tracking and impedance behavior. The most obvious example is certainly the standard PD (proportional-derivative) controller with feedforward of the desired joint-space trajectory. However, lower bounds for the PD gains are required in the stability analysis [4, 5], consequently limiting the capabilities of the controller for physical interaction with low impedance. The so-called *PD+* [6, 5] or *augmented* PD controller [1] features comparable properties in terms of preserving the natural dynamics, but it imposes no restrictions on the control gains. In regulation control, the notation *compliance control* is often used for such approaches where the natural inertia is deliberately kept [7]. In a PD+ implementation, the 'PD' part with constant control gains is augmented by a compensation term '+' that compensates for gravitational effects, and precompensates for expected inertial and Coriolis/centrifugal effects along a desired trajectory. In prac-

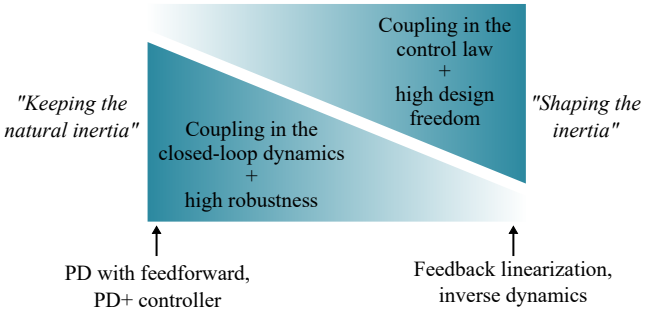

Figure 1: A qualitative representation of the preservation and active modification of the natural inertia in terms of the couplings related to the control law and the closed-loop dynamics.

*Corresponding author
Email addresses: alexander.dietrich@dlr.de (Alexander Dietrich), xuwei.wu@dlr.de (Xuwei Wu), kristin.bussmann@dlr.de (Kristin Bussmann), marie.harder@dlr.de (Marie Harder), maged.iskandar@dlr.de (Maged Iskandar), johannes.englsberger@dlr.de (Johannes Englsberger), christian.ott@dlr.de (Christian Ott), alin.albu-schaeffer@dlr.de (Alin Albu-Schäffer)

tice the PD+ is known to be particularly robust. However, the closed-loop dynamics remain nonlinear, and consequently, tools from linear control theory cannot be applied for the analysis of the closed-loop behavior.

1.1. State of the art and classification of controllers

Although the literature for tracking and interaction controllers in robotics is vast, most model-based approaches can be, more or less, placed in between these two fundamentally different concepts w. r. t. the treatment of the inertial behavior: the complete active shaping of the inertia (feedback linearization) versus the preservation of the natural one (e. g., PD with feedforward or PD+). An illustration is given in Fig. 1 which highlights the fact that a decoupled closed-loop behavior requires significant couplings in the control law, and vice versa. One example of a passivity-based controller is the adaptive approach by Slotine and Li [8], which exploits the structure of the natural nonlinear dynamics as classical PD+ control and can avoid joint acceleration measurements and the inverse of the inertia matrix. Either or both of these requirements are typical in computed-torque-based schemes [9, 10, 11]. As the natural inertia is conserved, the passivity-based approach [8] is located on the left side of Fig. 1. Staying in the figure, the path from the left to the right is taken in the comparison [12] between down-scaling of the natural inertia and its active diagonalization. In flexible-joint robots, the feedback linearization [13] achieves a fourth-order linear and decoupled system by means of full cancellation of the nonlinearities, while decoupling-based and backstepping approaches annihilate the couplings between the link-side and motor-side dynamics through partial feedback linearization [14, 7]. However, these approaches generally require the feedback of link-side variables up to jerks even for the regulation case. This restriction has been removed in the backstepping strategies [15, 16] by replacing the unavailable measurements with approximate differentiation but at the cost of additional gain tuning efforts and increased complexity of the control law. Passivity-based approaches have been developed in [17, 18, 19] motivated by an energetic point of view, resulting in improved robustness against model uncertainties [7]. Although the closed-loop systems with backstepping and passivity-based approaches can both be represented as interconnected passive subsystems [14], the motor-side subsystem in the case of backstepping does not provide an energetic interpretation and it is similar to the artificial passive system imposed by a feedback linearization in rigid-joint robots [20]. Among recent works, an approach is developed in [21, 22] on the basis of the classical feedback linearization [13], but it exploits the intrinsic passivity properties of the link-side dynamics to enhance the robustness; the control scheme proposed in [23] feedforward-compensates the link-side dynamics and feedback-linearizes the motor-side one, making it an extreme example from the right side of Fig. 1.

If the robot is controlled in task space such as in the Cartesian coordinates of the end-effector, various adaptations exist for both passivity-based and feedback linearization based approaches. The Operational Space Formulation (OSF) [24] is probably the most popular one in which the system is feedback-linearized. Extensions of OSF to multi-tasking control can be found in [25, 26, 27, 28], among others. Interestingly, it has been shown that these approaches are in fact equivalent to common inverse dynamics solutions [29]. In optimization-based control, the realization of desired linear closed-loop dynamics is often aimed at [30, 31]. However, the preservation of the natural, nonlinear inertial properties can also be found in the state of the art [32], yielding high robustness due to the passivity-based controller design. Task-space controllers based on PD+ strategies are also widely adopted in the literature [7] and commonly used on modern torque-controlled lightweight robots nowadays, and they have recently been extended to the hierarchical multi-tasking case [33], for example. In task-space haptic teleoperation the active reduction of the apparent inertia [34] is a standard approach due to its advantages in terms of fidelity and user transparency. In [12] a comparison between down-scaling of the natural inertia and its active diagonalization has been conducted. While the decoupling in the diagonalization is beneficial for the teleoperator's level of immersion, the apparent inertia can only be reduced by about 50 %, while the down-scaling of the natural inertia allows a reduction of about 67 %. In [26] the authors concluded that the control performance of OSF approaches degrades during fast motions if the identified inertia matrix is not highly accurate. These results indicate the tendency that the conservation of the natural inertia properties can be advantageous in terms of control performance and stability but it inevitably limits the options and possibilities during the control design.

1.2. Basis for a representative comparison: PD+ and feedback linearization

Both the PD+ and the feedback linearization (FL) as representatives for the keeping and shaping of the natural inertia, respectively, have been extensively but separately studied in the literature. Yet, no thorough comparison of the numerous properties and characteristics has been conducted so far. Furthermore, available analyses usually consider the pure motion control problem but neglect the physical interaction case [5], which becomes increasingly relevant for modern lightweight robots being operated close to or in contact with humans. Therefore, this article addresses the comparison of these two fundamentally different strategies and investigates the practical consequences on interaction and tracking control in case studies on a common torque-controlled lightweight robot. Due to the generality of the conclusions, the obtained insights are crucial for the target-oriented design of new robot controllers and the adequate choice of the appropriate control approach depending on the application scenarios and system conditions.

1.3. Structure

The article is organized as follows: After the recapitulation of the PD+ and FL controllers in Section 2, the theoretical comparison is conducted in Section 3. In Section 4, experiments on a commercially available torque-controlled lightweight robot verify the theory and complement the analysis from a practitioner's point of view. After the discussion in Section 5, the article is closed in Section 6.

2. Fundamentals

The rigid-body dynamics of a robot with n degrees of freedom (DOF) can be written as

$$\boldsymbol{M}(\boldsymbol{q})\ddot{\boldsymbol{q}} + \boldsymbol{C}(\boldsymbol{q},\dot{\boldsymbol{q}})\dot{\boldsymbol{q}} + \boldsymbol{g}(\boldsymbol{q}) = \boldsymbol{\tau} + \boldsymbol{\tau}_{\text{ext}} \tag{1}$$

with $\boldsymbol{q},\dot{\boldsymbol{q}},\ddot{\boldsymbol{q}} \in \mathbb{R}^n$ describing the joint positions, velocities, and accelerations, respectively. The symmetric and positive definite inertia matrix is denoted by $\boldsymbol{M}(\boldsymbol{q}) \in \mathbb{R}^{n\times n}$ and the Coriolis/centrifugal matrix is described by $\boldsymbol{C}(\boldsymbol{q},\dot{\boldsymbol{q}}) \in \mathbb{R}^{n\times n}$. The term $\boldsymbol{g}(\boldsymbol{q}) \in \mathbb{R}^n$ represents the generalized gravity forces based on the gravity potential $V_{\text{g}}(\boldsymbol{q})$ through $\boldsymbol{g}(\boldsymbol{q}) = (\partial V_{\text{g}}(\boldsymbol{q})/\partial \boldsymbol{q})^T$. The covectors $\boldsymbol{\tau},\boldsymbol{\tau}_{\text{ext}} \in \mathbb{R}^n$ stand for the generalized forces and external forces, respectively. The control input is $\boldsymbol{\tau}$. As of now, the following assumptions will be made:

Assumption 1. *The matrices $\boldsymbol{M}(\boldsymbol{q})$ and $\boldsymbol{C}(\boldsymbol{q},\dot{\boldsymbol{q}})$ are uniformly bounded for all $\boldsymbol{q}$, and $\boldsymbol{C}(\boldsymbol{q},\dot{\boldsymbol{q}})$ is linear in $\dot{\boldsymbol{q}}$.*

Remark 1. A complete classification of robots that satisfy Assumption 1 is presented in [35]. This classical condition applies, among others, to any robot with only revolute joints or such systems with free-floating bases or mounted on mobile platforms.

Assumption 2. *The matrix $\boldsymbol{C}(\boldsymbol{q},\dot{\boldsymbol{q}})$ fulfills the condition $\dot{\boldsymbol{M}}(\boldsymbol{q},\dot{\boldsymbol{q}}) = \boldsymbol{C}(\boldsymbol{q},\dot{\boldsymbol{q}}) + \boldsymbol{C}(\boldsymbol{q},\dot{\boldsymbol{q}})^T$.*

Remark 2. One can straightforwardly formulate $\boldsymbol{C}(\boldsymbol{q},\dot{\boldsymbol{q}})$ in a way such that Assumption 2 holds [1]. An interpretation of this condition is also given by the skew-symmetry of $\dot{\boldsymbol{M}}(\boldsymbol{q},\dot{\boldsymbol{q}}) - 2\boldsymbol{C}(\boldsymbol{q},\dot{\boldsymbol{q}})$ or the fact that the total energy $V(\boldsymbol{q},\dot{\boldsymbol{q}}) = \frac{1}{2}\dot{\boldsymbol{q}}^T\boldsymbol{M}(\boldsymbol{q})\dot{\boldsymbol{q}} + V_{\text{g}}(\boldsymbol{q})$ of the system (1) is constant for $\boldsymbol{\tau} = \boldsymbol{\tau}_{\text{ext}} = \boldsymbol{0}$, that is, $\dot{V} = 0$.

The control goals considered here are twofold:

- **Trajectory tracking**: realization of the desired trajectory in joint space with continuous and bounded functions $\boldsymbol{q}_{\text{d}}(t),\dot{\boldsymbol{q}}_{\text{d}}(t),\ddot{\boldsymbol{q}}_{\text{d}}(t) \in \mathbb{R}^n$ in time t.
- **Impedance behavior**: realization of user-specified, symmetric, positive definite interaction stiffness and damping matrices $\boldsymbol{K},\boldsymbol{D} \in \mathbb{R}^{n\times n}$.

Thus, the controller has to be capable of providing both highly dynamic trajectory tracking and dedicated interaction behavior at the same time. In the following analysis, the joint-space errors

$$\boldsymbol{e} = \boldsymbol{q} - \boldsymbol{q}_{\text{d}}(t) \tag{2}$$

and their time derivatives $\dot{\boldsymbol{e}},\ddot{\boldsymbol{e}}$ will be used.

2.1. PD+ / augmented PD control

The well known PD+ control law [6, 1, 5] is given by

$$\boldsymbol{\tau} = \underbrace{\boldsymbol{M}(\boldsymbol{q})\ddot{\boldsymbol{q}}_{\text{d}} + \boldsymbol{C}(\boldsymbol{q},\dot{\boldsymbol{q}})\dot{\boldsymbol{q}}_{\text{d}} + \boldsymbol{g}(\boldsymbol{q})}_{\text{“+” part}} \underbrace{-\boldsymbol{K}\boldsymbol{e} - \boldsymbol{D}\dot{\boldsymbol{e}}}_{\text{PD part}} . \tag{3}$$

The first two components in (3) cover the nominal joint torque to implement the desired trajectory (precompensation). The third element compensates for gravitational effects, and the PD part realizes the specified stiffness and damping. Strictly speaking, the “+” part in (3) is not a feedforward term since it involves measured states $\boldsymbol{q},\dot{\boldsymbol{q}}$ besides the desired trajectory profile, thus it should be rather interpreted as a dynamics compensation action. Inserting (3) into (1) yields the nonlinear closed-loop dynamics

$$\boldsymbol{M}(\boldsymbol{q})\ddot{\boldsymbol{e}} + (\boldsymbol{C}(\boldsymbol{q},\dot{\boldsymbol{q}}) + \boldsymbol{D})\,\dot{\boldsymbol{e}} + \boldsymbol{K}\boldsymbol{e} = \boldsymbol{\tau}_{\text{ext}} . \tag{4}$$

One characteristic property of (3) is that the PD part is largely decoupled w. r. t. the joints. No couplings related to the control feedback of $\boldsymbol{e}$ and $\dot{\boldsymbol{e}}$ are present at all if $\boldsymbol{K}$ and $\boldsymbol{D}$ are chosen diagonal. However, the closed-loop dynamics (4) contain considerable couplings, cf. Fig. 1.

2.2. Feedback linearization with feedback of $\boldsymbol{\tau}_{\text{ext}}$ (FL1)

The control law for the complete feedback linearization including feedback of $\boldsymbol{\tau}_{\text{ext}}$ is

$$\begin{aligned}\boldsymbol{\tau} = {} & \underbrace{\boldsymbol{C}(\boldsymbol{q},\dot{\boldsymbol{q}})\dot{\boldsymbol{q}} + \boldsymbol{g}(\boldsymbol{q}) - \boldsymbol{\tau}_{\text{ext}}}_{\text{Dynamics compensation}} + \underbrace{\boldsymbol{M}(\boldsymbol{q})\ddot{\boldsymbol{q}}_{\text{d}}}_{\text{Precompensation}} \\ & + \underbrace{\boldsymbol{M}(\boldsymbol{q})\boldsymbol{M}_{\text{d}}^{-1}\left(-\boldsymbol{K}\boldsymbol{e} - \boldsymbol{D}\dot{\boldsymbol{e}} + \boldsymbol{\tau}_{\text{ext}}\right)}_{\text{Enforcement of desired linear dynamics}}\end{aligned} \tag{5}$$

which will be denoted by FL1 in the following. The first three components in (5) annihilate the natural dynamics from (1), while $\boldsymbol{M}(\boldsymbol{q})\ddot{\boldsymbol{q}}_{\text{d}}$ precompensates for the generalized inertial forces required in the desired trajectory. The last term imposes the desired linear dynamic behavior with the desired symmetric and constant inertia matrix $\boldsymbol{M}_{\text{d}} \in \mathbb{R}^{n\times n}$. Consequently, the equations of motion of the closed loop take the form

$$\boldsymbol{M}_{\text{d}}\ddot{\boldsymbol{e}} + \boldsymbol{D}\dot{\boldsymbol{e}} + \boldsymbol{K}\boldsymbol{e} = \boldsymbol{\tau}_{\text{ext}} \tag{6}$$

and feature linear dynamics with constant coefficients. If $\boldsymbol{K}$, $\boldsymbol{D}$, and $\boldsymbol{M}_{\text{d}}$ are chosen diagonal, the joint dynamics are completely decoupled. However, in contrast to the PD+, the control law (5) features significant couplings among the joints due to the involvement of the nonlinear, configuration-dependent term $\boldsymbol{M}(\boldsymbol{q})\boldsymbol{M}_{\text{d}}^{-1}$, cf. Fig. 1.

2.3. Feedback linearization without feedback of $\boldsymbol{\tau}_{\text{ext}}$ (FL2)

An alternative to (5) is to avoid feedback of the measured/estimated generalized external forces $\boldsymbol{\tau}_{\text{ext}}$, that is,

$$\begin{aligned}\boldsymbol{\tau} = {} & \boldsymbol{C}(\boldsymbol{q},\dot{\boldsymbol{q}})\dot{\boldsymbol{q}} + \boldsymbol{g}(\boldsymbol{q}) + \boldsymbol{M}(\boldsymbol{q})\ddot{\boldsymbol{q}}_{\text{d}} \\ & + \boldsymbol{M}(\boldsymbol{q})\boldsymbol{M}_{\text{d}}^{-1}\left(-\boldsymbol{K}\boldsymbol{e} - \boldsymbol{D}\dot{\boldsymbol{e}}\right) .\end{aligned} \tag{7}$$

In this case, the closed-loop dynamics will slightly differ from (6) concerning the appearance of $\boldsymbol{\tau}_{\text{ext}}$:

$$\boldsymbol{M}_{\text{d}}\ddot{\boldsymbol{e}} + \boldsymbol{D}\dot{\boldsymbol{e}} + \boldsymbol{K}\boldsymbol{e} = \boldsymbol{M}_{\text{d}}\boldsymbol{M}(\boldsymbol{q})^{-1}\boldsymbol{\tau}_{\text{ext}} \ . \tag{8}$$

In the following, this type of feedback linearization will be denoted by FL2. It features linear dynamics during free motion ($\boldsymbol{\tau}_{\text{ext}} = \boldsymbol{0}$) but it shows nonlinear dynamics during interaction ($\boldsymbol{\tau}_{\text{ext}} \neq \boldsymbol{0}$). The case (7)–(8) applies in practice if external disturbances are ignored in the model (1) to be feedback-linearized. The frequent occurrence of this scenario in the literature [26] justifies the inclusion of FL2 in the following comparison but it is well known that a modified inertia perceived during physical interaction can only be achieved through explicit feedback of $\boldsymbol{\tau}_{\text{ext}}$ [7, 36].

3. Theoretical Comparison

In this section, the three controllers (PD+, FL1, FL2) will be briefly compared from a theoretical point of view. A condensed overview of the main properties is presented in Table 2 at the end of this section.

3.1. Tuning parameters in the control law

As the PD+ aims at the preservation of the natural inertia, the design choice in (3) reduces to the constant PD gains $\boldsymbol{K}$ and $\boldsymbol{D}$. This choice can be obviously motivated from a physical point of view, representing contact stiffness and damping.

The closed-loop dynamics (6) of FL1 require the specification of $\boldsymbol{K}$, $\boldsymbol{D}$, and $\boldsymbol{M}_{\text{d}}$. While there exist various ways to define these values, especially the following two are common for interaction and tracking control.

- Motivated by interaction behavior: The stiffness $\boldsymbol{K}$ and damping $\boldsymbol{D}$ can be set analogous to the PD+ case. Additionally, the constant desired inertia $\boldsymbol{M}_{\text{d}}$ needs to be specified. This physical motivation is particularly useful in interaction control, where the contact behavior and the inertial response are relevant.

- Motivated by tracking behavior: $2n$ constant poles[1] of the closed loop can be placed according to the desired oscillation frequencies and damping ratios. An additional type of parameter can be specified in the presence of external disturbances. For example, $\boldsymbol{M}_{\text{d}}$ can be set to obtain the desired inertial response to $\boldsymbol{\tau}_{\text{ext}}$ where $\boldsymbol{M}_{\text{d}} = \boldsymbol{I}$ represents a common choice. It has to be noted that this method implicitly results in a fixed value for $\boldsymbol{K}$. Alternatively, specifying $\boldsymbol{K}$ to limit the motion range due to external disturbances automatically assigns $\boldsymbol{M}_{\text{d}}$ [37].

In case of FL2 control, one can reformulate (8) to

$$\ddot{\boldsymbol{e}} + \boldsymbol{M}_{\text{d}}^{-1}\boldsymbol{D}\dot{\boldsymbol{e}} + \boldsymbol{M}_{\text{d}}^{-1}\boldsymbol{K}\boldsymbol{e} = \boldsymbol{M}(\boldsymbol{q})^{-1}\boldsymbol{\tau}_{\text{ext}} \ . \tag{9}$$

Although the three terms $\boldsymbol{M}_{\text{d}}, \boldsymbol{D}, \boldsymbol{K}$ can be set, there only exist two independent effective gains to tune: $\boldsymbol{M}_{\text{d}}^{-1}\boldsymbol{D}$ and $\boldsymbol{M}_{\text{d}}^{-1}\boldsymbol{K}$. In other words, the effective tuning parameters for FL2 control are merely the $2n$ constant poles, or equivalently, the ratios $\boldsymbol{M}_{\text{d}}^{-1}\boldsymbol{D}$ and $\boldsymbol{M}_{\text{d}}^{-1}\boldsymbol{K}$.

While the closed-loop poles for FL1 and FL2 are constant, the local[2] closed-loop poles in case of PD+ control are highly configuration-dependent. That is due to the nonlinear nature of (4) originating from $\boldsymbol{M}(\boldsymbol{q})$ and $\boldsymbol{C}(\boldsymbol{q}, \dot{\boldsymbol{q}})$. If that aspect is not considered in the gain design of PD+, one may encounter large local closed-loop poles which are infeasible due to practical limitations such as discretization effects, time delay, or limited torque dynamics. Therefore, the PD+ gains $\boldsymbol{K}$ and $\boldsymbol{D}$ are usually chosen in a way such that the robot shows a stable and effective interaction and tracking behavior in the entire workspace. In Section 4 (experiment #1c) it will be shown that instability can result in the PD+ controlled robot if $\boldsymbol{K}$ and $\boldsymbol{D}$ are naively taken from the pole placement approach of FL1/FL2 without consideration of these aspects.

It has to be noted that the realization of the desired pole placement and decoupling for FL1 and FL2 largely depend on the accuracy of the identified model. In practice there remain dynamic couplings especially when the system undergoes fast motion that involves a high number of joints, as will be shown in Section 4 (experiment #1d).

3.2. Passivity and stability

For physical interaction with the robot ($\boldsymbol{\tau}_{\text{ext}} \neq \boldsymbol{0}$), passivity properties are of major importance. The notion of passivity is classically defined for time-invariant systems only [38]. Besides the analysis of this case (regulation control), we will straightforwardly extend the definition to the time-varying case (tracking control). More details on passivity and the corresponding storage functions for time-varying systems can be found in [20]. Although the physical interpretation is not as intuitive as before since the involved storage functions do not represent the mechanical energy anymore, the overall properties can be transferred without loss of generality and give valuable insights into the dynamics of physical interaction. In free motion ($\boldsymbol{\tau}_{\text{ext}} = \boldsymbol{0}$), the stability properties can be investigated based on the same storage functions. Note that all statements on passivity and stability made in the following are globally valid.

As storage function for the PD+ controlled robot one can make the intuitive choice

$$S_{\text{PD+}} = \frac{1}{2}\dot{\boldsymbol{e}}^T\boldsymbol{M}(\boldsymbol{q})\dot{\boldsymbol{e}} + \frac{1}{2}\boldsymbol{e}^T\boldsymbol{K}\boldsymbol{e} \ , \tag{10}$$

$$\dot{S}_{\text{PD+}} = \dot{\boldsymbol{e}}^T\boldsymbol{\tau}_{\text{ext}} - \dot{\boldsymbol{e}}^T\boldsymbol{D}\dot{\boldsymbol{e}} \ , \tag{11}$$

[1] or two poles per joint, if a complete decoupling in joint space is desired.

[2] *Local* closed-loop poles mean the eigenvalues of the linearized controlled robot dynamics at each time instant.

using (4). For the regulation case ($\dot{\boldsymbol{q}}_\mathrm{d} = \ddot{\boldsymbol{q}}_\mathrm{d} = \boldsymbol{0}$), (10) simplifies to the real physical energy $\frac{1}{2}\dot{\boldsymbol{q}}^T\boldsymbol{M}(\boldsymbol{q})\dot{\boldsymbol{q}} + \frac{1}{2}\boldsymbol{e}^T\boldsymbol{K}\boldsymbol{e}$ as $\dot{\boldsymbol{e}} = \dot{\boldsymbol{q}}$ holds, i. e., the storage function involves the kinetic energy and the elastic potential described by the virtual spring with stiffness $\boldsymbol{K}$, similar to the task-space case described in [7]. The corresponding power transfer is expressed by $\dot{\boldsymbol{q}}^T\boldsymbol{\tau}_\mathrm{ext} - \dot{\boldsymbol{q}}^T\boldsymbol{D}\dot{\boldsymbol{q}}$ instead of (11). Note that the component $\dot{\boldsymbol{q}}^T\boldsymbol{\tau}_\mathrm{ext}$ equals the real physical power transmitted by the user during interaction. Consequently, both for the time-invariant and for the time-varying case, one can conclude passivity w. r. t. the storage function (10), the input $\boldsymbol{\tau}_\mathrm{ext}$, and the output $\dot{\boldsymbol{e}}$. In other words, $(\boldsymbol{\tau}_\mathrm{ext} \to \dot{\boldsymbol{e}})$ describes a passive mapping. For the interaction-free case ($\boldsymbol{\tau}_\mathrm{ext} = \boldsymbol{0}$), one can conclude stability of $\boldsymbol{e} = \dot{\boldsymbol{e}} = \boldsymbol{0}$ via (10)–(11) and equivalently boundedness of the states $\boldsymbol{q}, \dot{\boldsymbol{q}}$ for bounded desired profiles $\boldsymbol{q}_\mathrm{d}(t), \dot{\boldsymbol{q}}_\mathrm{d}(t)$. In order to prove exponential stability of $\boldsymbol{e} = \dot{\boldsymbol{e}} = \boldsymbol{0}$ the modified storage function

$$S_{\mathrm{PD+},\epsilon} = S_{\mathrm{PD+}} + \epsilon \cdot \dot{\boldsymbol{e}}^T\boldsymbol{M}(\boldsymbol{q})\boldsymbol{e} \tag{12}$$

with the small positive constant ϵ can be utilized. This choice can be interpreted as skewing of the level sets w. r. t. $S_{\mathrm{PD+}}$ [1]. One can show that there always exists an ϵ that renders $S_{\mathrm{PD+},\epsilon}$ a strict Lyapunov function [39] with its time derivative $\dot{S}_{\mathrm{PD+},\epsilon}$ being negative definite in $(\boldsymbol{e}, \dot{\boldsymbol{e}})$, thereby concluding exponential stability of $\boldsymbol{e} = \dot{\boldsymbol{e}} = \boldsymbol{0}$ [1]. However, it has to be noted that the decay rate obtained here has limited significance in practice as it is, in general, very conservative and depends on ϵ. Therefore, the practical interpretation of the above stability analysis is rather global asymptotic stability of $\boldsymbol{e} = \dot{\boldsymbol{e}} = \boldsymbol{0}$ than global exponential stability.

Similar to (10) one can define a storage function

$$S_{\mathrm{FL1}} = \frac{1}{2}\dot{\boldsymbol{e}}^T\boldsymbol{M}_\mathrm{d}\dot{\boldsymbol{e}} + \frac{1}{2}\boldsymbol{e}^T\boldsymbol{K}\boldsymbol{e} \ , \tag{13}$$

$$\dot{S}_{\mathrm{FL1}} = \dot{\boldsymbol{e}}^T\boldsymbol{\tau}_\mathrm{ext} - \dot{\boldsymbol{e}}^T\boldsymbol{D}\dot{\boldsymbol{e}} \ , \tag{14}$$

for FL1 using (6). Note that the inertia $\boldsymbol{M}_\mathrm{d}$ is used in (13) instead of $\boldsymbol{M}(\boldsymbol{q})$ as done in (4). Yet, the powers (11) and (14) are identical. Consequently, one can conclude similar passivity properties as for the PD+ controller. Both for the time-invariant and for the time-varying case one can conclude passivity of FL1 w. r. t. the storage function (13), the input $\boldsymbol{\tau}_\mathrm{ext}$, and the output $\dot{\boldsymbol{e}}$. As above, $(\boldsymbol{\tau}_\mathrm{ext} \to \dot{\boldsymbol{e}})$ describes a passive mapping. Although this strong and beneficial statement on passivity can be made for FL1, it has to be noted that this theoretical result can have limited applicability and validity in practice. As analyzed in [40], "*when a controller attempts to emulate dynamics that differ significantly from the intrinsic hardware dynamics, an increased risk of coupled or contact instability arises*". That effect has been explained by means of passivity in [41], showing that when the desired inertia significantly differs from the natural one, a non-passive behavior can be obtained in practice as a result of resonant modes between the sensor and actuator [42]. Furthermore, differences between the theory and implementation on hardware can also be traced back to discretization, time delays, actuator and sensor limitations, and unmodeled dynamics [40]. In the interaction-free case ($\boldsymbol{\tau}_\mathrm{ext} = \boldsymbol{0}$), the closed-loop dynamics (6) for FL1 reduce to

$$\boldsymbol{M}_\mathrm{d}\ddot{\boldsymbol{e}} + \boldsymbol{D}\dot{\boldsymbol{e}} + \boldsymbol{K}\boldsymbol{e} = \boldsymbol{0} \ . \tag{15}$$

Due to the constant coefficients $\boldsymbol{M}_\mathrm{d}, \boldsymbol{D}, \boldsymbol{K}$, one can straightforwardly conclude exponential stability of the equilibrium $\boldsymbol{e} = \dot{\boldsymbol{e}} = \boldsymbol{0}$ [2].

To analyze the passivity properties of FL2, one can proceed analogously as in (14) to obtain

$$S_{\mathrm{FL2}} = \frac{1}{2}\dot{\boldsymbol{e}}^T\boldsymbol{M}_\mathrm{d}\dot{\boldsymbol{e}} + \frac{1}{2}\boldsymbol{e}^T\boldsymbol{K}\boldsymbol{e} \ , \tag{16}$$

$$\dot{S}_{\mathrm{FL2}} = \dot{\boldsymbol{e}}^T\boldsymbol{M}_\mathrm{d}\boldsymbol{M}(\boldsymbol{q})^{-1}\boldsymbol{\tau}_\mathrm{ext} - \dot{\boldsymbol{e}}^T\boldsymbol{D}\dot{\boldsymbol{e}} \ , \tag{17}$$

using (8). One can observe that the conclusion of passivity properties cannot be straightforwardly made due to the distortion of $\boldsymbol{\tau}_\mathrm{ext}$ by the configuration-dependent factor $\boldsymbol{M}_\mathrm{d}\boldsymbol{M}(\boldsymbol{q})^{-1}$ originating from (8). Consequently, $\dot{\boldsymbol{e}}^T\boldsymbol{\tau}_\mathrm{ext}$ (or $\dot{\boldsymbol{q}}^T\boldsymbol{\tau}_\mathrm{ext}$ in the regulation case) transmitted by the user or the environment during physical interaction is not identical to the power entering the closed-loop dynamics during interaction when considering the physically motivated, intuitive storage function (16). The interaction-free case for FL2 is identical to the one of FL1 since (6) equals (8) for $\boldsymbol{\tau}_\mathrm{ext} = \boldsymbol{0}$. Therefore, exponential stability of the equilibrium $\boldsymbol{e} = \dot{\boldsymbol{e}} = \boldsymbol{0}$ can be stated for FL2.

It is important to mention that a passive closed-loop behavior can be safety-critical during physical contact. The environment can be usually represented as a passive mapping $(\dot{\boldsymbol{q}} \to -\boldsymbol{\tau}_\mathrm{ext})$ [3, 18]. When (feedback-inter)connecting a controlled robot with passive mapping $(\boldsymbol{\tau}_\mathrm{ext} \to \dot{\boldsymbol{q}})$ with the environment, another passive system results. In other words, the controlled robot will not generate energy in the physical contact. For the regulation case of PD+ and FL1 that holds true. However, this statement, in turn, requires that (11) and (14) are actually achieved. For FL1 in practical settings, that is often not the case, e. g., an infeasible choice of $\boldsymbol{M}_\mathrm{d}$ may render (14) invalid in reality, leading to a loss of passivity and the consequence of contact instability [40], as described above.

3.3. Contact stiffness and perceived inertia

On the one hand, the stiffness is essential for physical interaction with humans or the environment as it defines the contact behavior. This property can be analyzed via the *static deviation* as a result of an interaction through $\boldsymbol{\tau}_\mathrm{ext}$. On the other hand, the perceived inertia also has significant influence on the physical interaction behavior. One can identify the latter by means of the instantaneous *inertial response* to $\boldsymbol{\tau}_\mathrm{ext}$ out of a static equilibrium. The conditions for these two cases are defined as follows:

- Conditions for *static deviation* to analyse the contact stiffness: $\dot{\boldsymbol{q}} = \ddot{\boldsymbol{q}} = \dot{\boldsymbol{q}}_\mathrm{d} = \ddot{\boldsymbol{q}}_\mathrm{d} = \boldsymbol{0}$.

- Conditions for *inertial response* to analyse the perceived inertia: $\boldsymbol{e} = \dot{\boldsymbol{e}} = \dot{\boldsymbol{q}}_\mathrm{d} = \ddot{\boldsymbol{q}}_\mathrm{d} = \boldsymbol{0}$.

The closed-loop dynamics with PD+ control simplify to

$$\text{Contact stiffness (PD+): } \boldsymbol{K}\boldsymbol{e} = \boldsymbol{\tau}_\mathrm{ext} \tag{18}$$
$$\text{Perceived inertia (PD+): } \boldsymbol{M}(\boldsymbol{q})\ddot{\boldsymbol{q}} = \boldsymbol{\tau}_\mathrm{ext} \tag{19}$$

and reveal the contact stiffness $\boldsymbol{K}$ and the perceived natural inertia $\boldsymbol{M}(\boldsymbol{q})$. For FL1 control, the closed-loop dynamics simplify to

$$\text{Contact stiffness (FL1): } \boldsymbol{K}\boldsymbol{e} = \boldsymbol{\tau}_\mathrm{ext} \tag{20}$$
$$\text{Perceived inertia (FL1): } \boldsymbol{M}_\mathrm{d}\ddot{\boldsymbol{q}} = \boldsymbol{\tau}_\mathrm{ext} \tag{21}$$

and show that the stiffness $\boldsymbol{K}$ and the inertia $\boldsymbol{M}_\mathrm{d}$ will be perceived during physical interaction with the robot. However, controlling the robot via FL2 leads to

$$\text{Contact stiffness (FL2): } \boldsymbol{M}(\boldsymbol{q})\boldsymbol{M}_\mathrm{d}^{-1}\boldsymbol{K}\boldsymbol{e} = \boldsymbol{\tau}_\mathrm{ext} \tag{22}$$
$$\text{Perceived inertia (FL2): } \boldsymbol{M}(\boldsymbol{q})\ddot{\boldsymbol{q}} = \boldsymbol{\tau}_\mathrm{ext}\ . \tag{23}$$

The effective stiffness $\boldsymbol{M}(\boldsymbol{q})\boldsymbol{M}_\mathrm{d}^{-1}\boldsymbol{K}$ obtained in (22) is a distorted version of the user-specified term $\boldsymbol{K}$. Due to the occurrence of $\boldsymbol{M}(\boldsymbol{q})$ it is highly configuration-dependent. Moreover, $\boldsymbol{K} \succ 0$ does not imply $\boldsymbol{M}(\boldsymbol{q})\boldsymbol{M}_\mathrm{d}^{-1}\boldsymbol{K} \succ 0$. Therefore, inertia shaping without feedback of $\boldsymbol{\tau}_\mathrm{ext}$ can lead to a negative contact stiffness and ultimately to contact instability in practice. The fact that the perceived inertia in (23) is $\boldsymbol{M}(\boldsymbol{q})$ instead of $\boldsymbol{M}_\mathrm{d}$ is not surprising, since it is well known that inertia shaping under physical interaction strictly requires feedback of $\boldsymbol{\tau}_\mathrm{ext}$ [7, 36].

3.4. Influence of modeling uncertainties

A practically relevant aspect in the controlled robot is how non-parametric model uncertainties, such as neglected joint frictions, motor dynamics, or measurement noise, will influence the closed-loop behavior. Therefore, we assume an additional term $\boldsymbol{\tau}_\mathrm{nonpar} \in \mathbb{R}^n$ appearing on the right-hand side of (1) which represents a generic unknown joint torque caused by non-parametric model uncertainties:

$$\boldsymbol{M}(\boldsymbol{q})\ddot{\boldsymbol{q}} + \boldsymbol{C}(\boldsymbol{q},\dot{\boldsymbol{q}})\dot{\boldsymbol{q}} + \boldsymbol{g}(\boldsymbol{q}) = \boldsymbol{\tau} + \boldsymbol{\tau}_\mathrm{ext} + \boldsymbol{\tau}_\mathrm{nonpar}\ . \tag{24}$$

As a result, the nominal closed-loop dynamics are affected by the disturbance terms

$$\boldsymbol{\gamma}_\mathrm{PD+,nonpar} = \boldsymbol{\tau}_\mathrm{nonpar}\ , \tag{25}$$
$$\boldsymbol{\gamma}_\mathrm{FL1,nonpar} = \boldsymbol{M}_\mathrm{d}\boldsymbol{M}(\boldsymbol{q})^{-1}\boldsymbol{\tau}_\mathrm{nonpar}\ , \tag{26}$$
$$\boldsymbol{\gamma}_\mathrm{FL2,nonpar} = \boldsymbol{M}_\mathrm{d}\boldsymbol{M}(\boldsymbol{q})^{-1}\boldsymbol{\tau}_\mathrm{nonpar}\ , \tag{27}$$

appearing on the right-hand sides of (4), (6), and (8), respectively. The effect of $\boldsymbol{\tau}_\mathrm{nonpar}$ is conserved in the case of PD+ as it appears unchanged, but the pre-multiplication of $\boldsymbol{\tau}_\mathrm{nonpar}$ by the coefficient $\boldsymbol{M}_\mathrm{d}\boldsymbol{M}(\boldsymbol{q})^{-1}$ changes its original effect in the closed-loop dynamics of FL1 and FL2.

In the following, unmodeled viscous joint friction shall serve as an example of $\boldsymbol{\tau}_\mathrm{nonpar}$, that is $\boldsymbol{\tau}_\mathrm{nonpar} = -\boldsymbol{D}_\mathrm{fric}\dot{\boldsymbol{q}}$ with the positive definite matrix $\boldsymbol{D}_\mathrm{fric} \in \mathbb{R}^{n\times n}$ containing the friction coefficients. The analysis of the time derivatives $\dot{S}_\mathrm{PD+}$ and $\dot{S}_\mathrm{FL1}$ of the respective physically motivated storage functions for the regulation case provides an intuitive interpretation of the practical effect of $\boldsymbol{\tau}_\mathrm{nonpar}$:

$$\dot{S}_\mathrm{PD+} = \dot{\boldsymbol{q}}^T\boldsymbol{\tau}_\mathrm{ext} - \dot{\boldsymbol{q}}^T\left(\boldsymbol{D} + \boldsymbol{D}_\mathrm{fric}\right)\dot{\boldsymbol{q}}\ , \tag{28}$$
$$\dot{S}_\mathrm{FL1} = \dot{\boldsymbol{q}}^T\boldsymbol{\tau}_\mathrm{ext} - \dot{\boldsymbol{q}}^T\boldsymbol{D}\dot{\boldsymbol{q}} - \dot{\boldsymbol{q}}^T\boldsymbol{M}_\mathrm{d}\boldsymbol{M}(\boldsymbol{q})^{-1}\boldsymbol{D}_\mathrm{fric}\dot{\boldsymbol{q}}\ . \tag{29}$$

Equation (28) shows that the term $-\dot{\boldsymbol{q}}^T\boldsymbol{D}_\mathrm{fric}\dot{\boldsymbol{q}}$ supports the passivity properties of PD+ and leads to additional dissipation, as also described by the dissipative nature of joint friction itself. That does not apply to (29) because the matrix $\boldsymbol{M}_\mathrm{d}\boldsymbol{M}(\boldsymbol{q})^{-1}\boldsymbol{D}_\mathrm{fric}$ is not necessarily positive definite. It can potentially even destabilize the closed-loop dynamics as discussed in [33]. One can proceed analogously for FL2 as done for FL1 to obtain similar implications. In general, all unmodeled parasitic effects are altered by the nonlinear, configuration-dependent coefficient $\boldsymbol{M}_\mathrm{d}\boldsymbol{M}(\boldsymbol{q})^{-1}$ in case of FL1 and FL2.

On the other hand, one can account for parametric model uncertainties in the analysis of the closed-loop behavior by using the estimated dynamic quantities[3] $\hat{\boldsymbol{M}}(\boldsymbol{q}), \hat{\boldsymbol{C}}(\boldsymbol{q},\dot{\boldsymbol{q}})$, and $\hat{\boldsymbol{g}}(\boldsymbol{q})$ in the control laws (3), (5), and (7). The parametric modeling errors can be formulated as:

$$\tilde{\boldsymbol{M}}(\boldsymbol{q}) = \hat{\boldsymbol{M}}(\boldsymbol{q}) - \boldsymbol{M}(\boldsymbol{q})\ , \tag{30}$$
$$\tilde{\boldsymbol{C}}(\boldsymbol{q},\dot{\boldsymbol{q}}) = \hat{\boldsymbol{C}}(\boldsymbol{q},\dot{\boldsymbol{q}}) - \boldsymbol{C}(\boldsymbol{q},\dot{\boldsymbol{q}})\ , \tag{31}$$
$$\tilde{\boldsymbol{g}}(\boldsymbol{q}) = \hat{\boldsymbol{g}}(\boldsymbol{q}) - \boldsymbol{g}(\boldsymbol{q})\ . \tag{32}$$

In the following, dependencies on $\boldsymbol{q}, \dot{\boldsymbol{q}}$ are omitted in the notations for the sake of clarity. The nominal closed-loop dynamics are influenced by disturbance terms appearing on the right-hand sides of (4), (6), and (8), respectively:[4]

$$\boldsymbol{\gamma}_\mathrm{PD+,par} = \tilde{\boldsymbol{M}}\ddot{\boldsymbol{q}}_\mathrm{d} + \tilde{\boldsymbol{C}}\dot{\boldsymbol{q}}_\mathrm{d} + \tilde{\boldsymbol{g}}\ , \tag{33}$$
$$\boldsymbol{\gamma}_\mathrm{FL1,par} = \boldsymbol{\gamma}_\mathrm{FL2,par} + \boldsymbol{M}_\mathrm{d}\boldsymbol{M}^{-1}\tilde{\boldsymbol{M}}\boldsymbol{M}_\mathrm{d}^{-1}\boldsymbol{\tau}_\mathrm{ext}\ , \tag{34}$$
$$\begin{aligned}\boldsymbol{\gamma}_\mathrm{FL2,par} = {}& \boldsymbol{M}_\mathrm{d}\boldsymbol{M}^{-1}(\tilde{\boldsymbol{M}}\ddot{\boldsymbol{q}}_\mathrm{d} + \tilde{\boldsymbol{C}}\dot{\boldsymbol{q}} + \tilde{\boldsymbol{g}}) \\ & + \boldsymbol{M}_\mathrm{d}\boldsymbol{M}^{-1}\tilde{\boldsymbol{M}}\boldsymbol{M}_\mathrm{d}^{-1}(-\boldsymbol{K}\boldsymbol{e} - \boldsymbol{D}\dot{\boldsymbol{e}})\ .\end{aligned} \tag{35}$$

Note that the influence of $\boldsymbol{\gamma}_\mathrm{PD+,par}$ is rather limited in practice. Although the first two terms in (33) depend on the actual states $\boldsymbol{q}, \dot{\boldsymbol{q}}$, they basically describe the common influence of feedforward errors in combination with modeling uncertainties. If the regulation case is considered, for example, then (33) boils down to inaccurate gravity compensation. The feedback linearizations FL1 and FL2 show a potentially more critical influence of modeling errors. Similar to the previous discussion of non-parametric uncertainties, the impact of modeling errors in FL1 and

[3] Without loss of generality we only consider uncertainties of dynamic parameters in this work.

[4] under the assumption of ideal feedback of $\boldsymbol{\tau}_\mathrm{ext}$. The analysis of error propagations related to $\boldsymbol{\tau}_\mathrm{ext}$ is conducted in Section 3.5.

FL2 can be amplified through $\boldsymbol{M}_\mathrm{d}\boldsymbol{M}(\boldsymbol{q})^{-1}$. Furthermore, even in the regulation case, the ideal closed-loop dynamics can be affected by disturbances that depend on $\dot{\boldsymbol{q}}$. In view of (34), the feedback of $\boldsymbol{\tau}_\mathrm{ext}$ in case of FL1 can also be distorted due to modeling errors. That acts as an additional disturbance term even with ideal feedback of $\boldsymbol{\tau}_\mathrm{ext}$.

3.5. Propagation of errors in the feedback of $\boldsymbol{\tau}_\mathrm{ext}$

It is well known that the feedback of external forces and torques (FL1) can be problematic regarding availability and accuracy of these quantities. Therefore, it is highly relevant in practice how inaccuracies affect the closed-loop dynamics. To analyze the propagation of errors in these terms, one can analyze (5) for the case that the term $\boldsymbol{\tau}_\mathrm{ext}$ is actually only an estimate $\hat{\boldsymbol{\tau}}_\mathrm{ext}$ which invovles the real disturbance $\boldsymbol{\tau}_\mathrm{ext}$ and the error $\tilde{\boldsymbol{\tau}}_\mathrm{ext}$:

$$\hat{\boldsymbol{\tau}}_\mathrm{ext} = \boldsymbol{\tau}_\mathrm{ext} + \tilde{\boldsymbol{\tau}}_\mathrm{ext} \ . \tag{36}$$

Applying the FL1 control law in consideration of (36) yields

$$\boldsymbol{M}_\mathrm{d}\ddot{\boldsymbol{e}} + \boldsymbol{D}\dot{\boldsymbol{e}} + \boldsymbol{K}\boldsymbol{e} = \boldsymbol{\tau}_\mathrm{ext} + \underbrace{\left(\boldsymbol{I} - \boldsymbol{M}_\mathrm{d}\boldsymbol{M}(\boldsymbol{q})^{-1}\right)\tilde{\boldsymbol{\tau}}_\mathrm{ext}}_{\text{Effective error}} \ . \tag{37}$$

Now one can observe the propagation of errors originating from the feedback of the measured/estimated external forces and torques. The "closer" the desired inertia $\boldsymbol{M}_\mathrm{d}$ and the natural one $\boldsymbol{M}(\boldsymbol{q})$ are, the smaller the influence of $\tilde{\boldsymbol{\tau}}_\mathrm{ext}$ is. If $\boldsymbol{M}_\mathrm{d} = \boldsymbol{M}(\boldsymbol{q})$, the term $\tilde{\boldsymbol{\tau}}_\mathrm{ext}$ will have no effect in (37) at all.[5] Since the desired inertia in FL1 is kept constant, significant differences between $\boldsymbol{M}_\mathrm{d}$ and $\boldsymbol{M}(\boldsymbol{q})$ can arise in the workspace of the robot which can amplify the effect of $\tilde{\boldsymbol{\tau}}_\mathrm{ext}$. An example is shown in Fig. 2. The constant joint positions $\boldsymbol{q}^*$ which determine $\boldsymbol{M}_\mathrm{d} = \boldsymbol{M}(\boldsymbol{q}^*)$ are illustrated in the left picture. This configuration describes an exemplary standard pose in the workspace of the robot where it is usually operated since the Jacobian matrix w. r. t. the six Cartesian end-effector coordinates has proper singular values and manipulability measure [43]. For the following analysis, an error of $\tilde{\boldsymbol{\tau}}_\mathrm{ext} = (1,0,0,0,0,0,0)^T\,\mathrm{Nm}$ is assumed. To investigate the effect of $\tilde{\boldsymbol{\tau}}_\mathrm{ext}$ in FL1, its instantaneous influence on the accelerations is analyzed, that is, (37) is rewritten as

$$\ddot{\boldsymbol{e}} = (\boldsymbol{M}_\mathrm{d}^{-1} - \boldsymbol{M}(\boldsymbol{q})^{-1})\tilde{\boldsymbol{\tau}}_\mathrm{ext} + \boldsymbol{M}_\mathrm{d}^{-1}(\boldsymbol{\tau}_\mathrm{ext} - \boldsymbol{D}\dot{\boldsymbol{e}} - \boldsymbol{K}\boldsymbol{e}) \tag{38}$$

and the mapping from $\tilde{\boldsymbol{\tau}}_\mathrm{ext}$ to $\ddot{\boldsymbol{e}}$ is examined by means of the corresponding amplification factor $(\boldsymbol{M}_\mathrm{d}^{-1} - \boldsymbol{M}(\boldsymbol{q})^{-1})$. While the effect is, by definition, zero in the left configuration, the other two configurations on the right result in large accelerations up to almost $90\,\mathrm{rad/s^2}$ in two joints. This excessive actuation in the first and third joint can be intuitively traced back to the small inertia of the second link in the "upright" configuration of the manipulator or the inversion of $\boldsymbol{M}(\boldsymbol{q})$ in (38), respectively. Note that in the joint configuration on the right-hand side in Fig. 2, the single estimation error of 1 Nm in the first joint leads to a resulting effective error torque of $(-88,-13,-27,14,-1,0,0)^T\,\mathrm{Nm}$. Without feedback of $\boldsymbol{\tau}_\mathrm{ext}$, as in the PD+ and FL2 cases, there is no such effect at all.

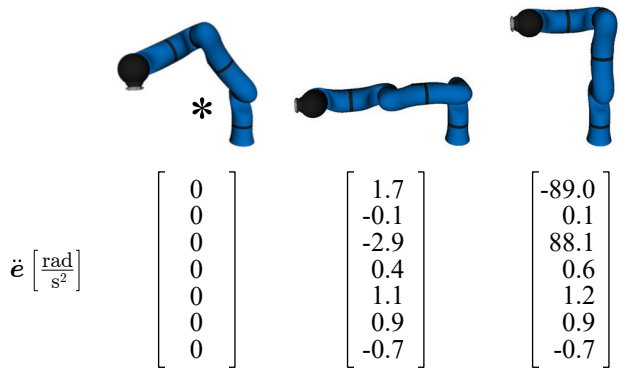

Figure 2: Error acceleration with FL1 due to inaccuracies in the feedback of $\boldsymbol{\tau}_\mathrm{ext}$ at the example of $\tilde{\boldsymbol{\tau}}_\mathrm{ext} = (1,0,0,0,0,0,0)^T\,\mathrm{Nm}$. The configuration $\boldsymbol{q}^*$ (marked by *) corresponds to the desired inertia $\boldsymbol{M}_\mathrm{d} = \boldsymbol{M}(\boldsymbol{q}^*)$.

3.6. Configuration-dependent scaling of the control gains for feedback quantities

All three control laws (3), (5), and (7) can be rewritten in a form where the effective control gains for $\boldsymbol{e}$ and $\dot{\boldsymbol{e}}$ are separated, as summarized in the first two columns of Table 1. While the gains in case of PD+ control are constant and represent the stiffness and damping parametrization, both FL1 and FL2 involve configuration-dependent terms. Similar to the discussion in Section 3.3, $\boldsymbol{M}(\boldsymbol{q})\boldsymbol{M}_\mathrm{d}^{-1}$ can have a large influence in practice. In [26] it is stated that one of the main reasons for the degraded control performance of OSF approaches during highly dynamic motions is an imprecise model of $\boldsymbol{M}(\boldsymbol{q})$ and its "*pre-multiplication of negative feedback terms*". The latter also applies to the control laws of FL1 and FL2.

The feedback action w. r. t. the tracking errors might be significantly increased or reduced in the case of FL1/FL2, depending on the eigenvectors and eigenvalues of $\boldsymbol{M}(\boldsymbol{q})\boldsymbol{M}_\mathrm{d}^{-1}$. In the experimental part (Section 4), an example will be shown wherein the gains in specific directions are increased by more than 340 %. Although the closed-loop dynamics (6) and (8) exhibit an ideal behavior in theory, an excessive scaling can be problematic in practice (reaching of torque limits, for example) and might ultimately destabilize the closed loop as it will also be demonstrated in the experiments. Moreover, the reduction of the feedback control gains in other directions (e. g., 90 % reduction in the experiments) can render the system insensitive to particular error combinations.

[5] Note that $\boldsymbol{M}_\mathrm{d} = \boldsymbol{M}(\boldsymbol{q})$ implies that no feedback of external torques is present in (5). Thus, no errors can be propagated.

Table 1: Effective control gains for feedback quantities

	$\boldsymbol{e}$	$\dot{\boldsymbol{e}}$	$\boldsymbol{\tau}_{\text{ext}}$
PD+	$-\boldsymbol{K}$	$-\boldsymbol{D}$	
FL1	$-\boldsymbol{M}(\boldsymbol{q})\boldsymbol{M}_{\text{d}}^{-1}\boldsymbol{K}$	$-\boldsymbol{M}(\boldsymbol{q})\boldsymbol{M}_{\text{d}}^{-1}\boldsymbol{D}$	$\boldsymbol{M}(\boldsymbol{q})\boldsymbol{M}_{\text{d}}^{-1}-\boldsymbol{I}$
FL2	$-\boldsymbol{M}(\boldsymbol{q})\boldsymbol{M}_{\text{d}}^{-1}\boldsymbol{K}$	$-\boldsymbol{M}(\boldsymbol{q})\boldsymbol{M}_{\text{d}}^{-1}\boldsymbol{D}$	

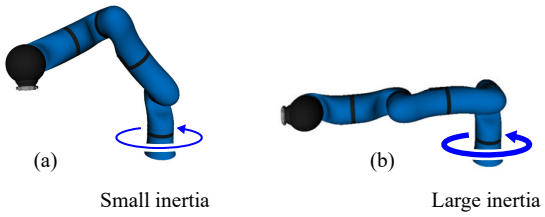

Figure 3: Comparison of different inertias w. r. t. the first joint. (a) configuration $\boldsymbol{q}^*$ with inertia $\boldsymbol{M}_{\text{d}} = \boldsymbol{M}(\boldsymbol{q}^*)$; (b) configuration $\boldsymbol{q}(T)$ with inertia $\boldsymbol{M}(\boldsymbol{q}(T))$ at time $t = T$.

One can isolate the feedback control gain for $\boldsymbol{\tau}_{\text{ext}}$ in the FL1 control law (5), as shown in Table 1. Even in case of accurate feedback of $\boldsymbol{\tau}_{\text{ext}}$, which implies $\tilde{\boldsymbol{\tau}}_{\text{ext}} = \boldsymbol{0}$, the active scaling of the apparent inertia can lead to infeasible commanded joint torques. An intuitive example is illustrated in Fig. 3 utilizing the first two configurations from Fig. 2. Analogously, (a) depicts the configuration $\boldsymbol{q}^*$ that determines $\boldsymbol{M}_{\text{d}} = \boldsymbol{M}(\boldsymbol{q}^*)$, while (b) shows the configuration $\boldsymbol{q}(T)$ at the current time instant T to be investigated. One can intuitively see that the inertia about the axis of the first joint (vertical) is larger in $\boldsymbol{q}(T)$ than in $\boldsymbol{q}^*$. Hence, when interacting with the robot in (b), the physical inertia has to be actively reduced in case of FL1 to achieve the same inertial response as in (a). In the example at hand, the eigenvalues of this gain matrix $\boldsymbol{M}(\boldsymbol{q}(T))\boldsymbol{M}(\boldsymbol{q}^*)^{-1} - \boldsymbol{I}$ are in the range between -0.5 and 6.4. Assuming an isolated external interaction of 20 Nm exerted on the first joint, for example, one obtains

$$\left(\boldsymbol{M}(\boldsymbol{q}(T))\boldsymbol{M}(\boldsymbol{q}^*)^{-1} - \boldsymbol{I}\right) \begin{pmatrix} 20 \\ 0 \\ 0 \\ 0 \\ 0 \\ 0 \\ 0 \end{pmatrix} \text{Nm} \approx \begin{pmatrix} 123.7 \\ -15.2 \\ -1.4 \\ 7.4 \\ -0.9 \\ -0.1 \\ -0.5 \end{pmatrix} \text{Nm} \ . \tag{39}$$

Besides the cross-couplings in the other joints, the excessive amplification from 20 Nm (measured/estimated) to almost 124 Nm (fed back) in the first joint can lead to problems concerning feasibility of the commanded joint torques. Two common examples are:

- The model (1) assumes an unrestricted torque range for the commanded torque $\boldsymbol{\tau}$. Joint torque limits exist in practice.
- The model (1) assumes an ideal torque source $\boldsymbol{\tau}$. If an underlying joint torque controller is utilized to provide this control input, such as in most torque-controlled lightweight robots [18], a limited bandwidth has to be considered.

Both exemplary cases can lead to large deviations between the dynamic model (1) and the hardware, jeopardizing the performance or the stability of the closed loop.

Note that there exist quadratic programming (QP) based control methods which explicitly consider actuation limits, e. g., in [44, 32]. However, such constraint-aware QP formulations usually jeopardize passivity considerations and guarantees, if applicable at all.

4. Experimental Comparison

The experiments are conducted on a commercially available KUKA LWR IV+ robot [45] with seven revolute DOF as shown in Fig. 17. Although (1) is commonly used on such systems, they actually belong to the class of elastic-joint robots where an underlying torque controller is employed to actively scale down the apparent motor inertia, reduce the effect of motor friction, and provide the torque interface $\boldsymbol{\tau}$ to be accessed in (1). No additional friction identification and compensation algorithm is used since the downscaling of the apparent joint motor inertias by factors in the range of 4.5–8.2 implicitly results in the reduction of motor friction effects by the same amount [46]. Moreover, as justified in [47], joint damping and link-side friction can be neglected for robots such as the one used here. This underlying controller [18, 46] runs in a 3 kHz loop and requires feedback of the measured joint torques. The controller parameters are set by the manufacturer KUKA and describe the default setup. The rigid-body outer loop to control (1) via PD+/FL1/FL2 runs at 1 kHz. It has to be noted that motor-side positions/velocities instead of the link-side coordinates are used in the outer loop in practice. The assumption of (1) can be justified with the large stiffness in the joints of the considered KUKA LWR IV+. The dynamic model is based on the data provided by the manufacturer and internal CAD data. Moreover, both the model of the inertia matrix and the gravity terms have been empirically updated to better match the specific characteristics of this particular system. For more information on the dynamic parameters of such manipulators the reader is referred to [48].

In the following experiments, the external torques are estimated through the widely used momentum-based disturbance observer [49] with an observer gain of $40\,\text{s}^{-1}$.[6] The case studies contain several parts. First, the control performance for trajectory tracking in free motion is investigated (experiments #1a - #1e). Afterwards, the contact behavior is analyzed during interaction between the robot and its environment (experiments #2a - #2c). For the sake of overview, Table 3 briefly describes all experiments.

[6] As analyzed in [47], typical and practical values of the observer gain in such torque-controlled robots are between $25\,\text{s}^{-1}$ and $75\,\text{s}^{-1}$.

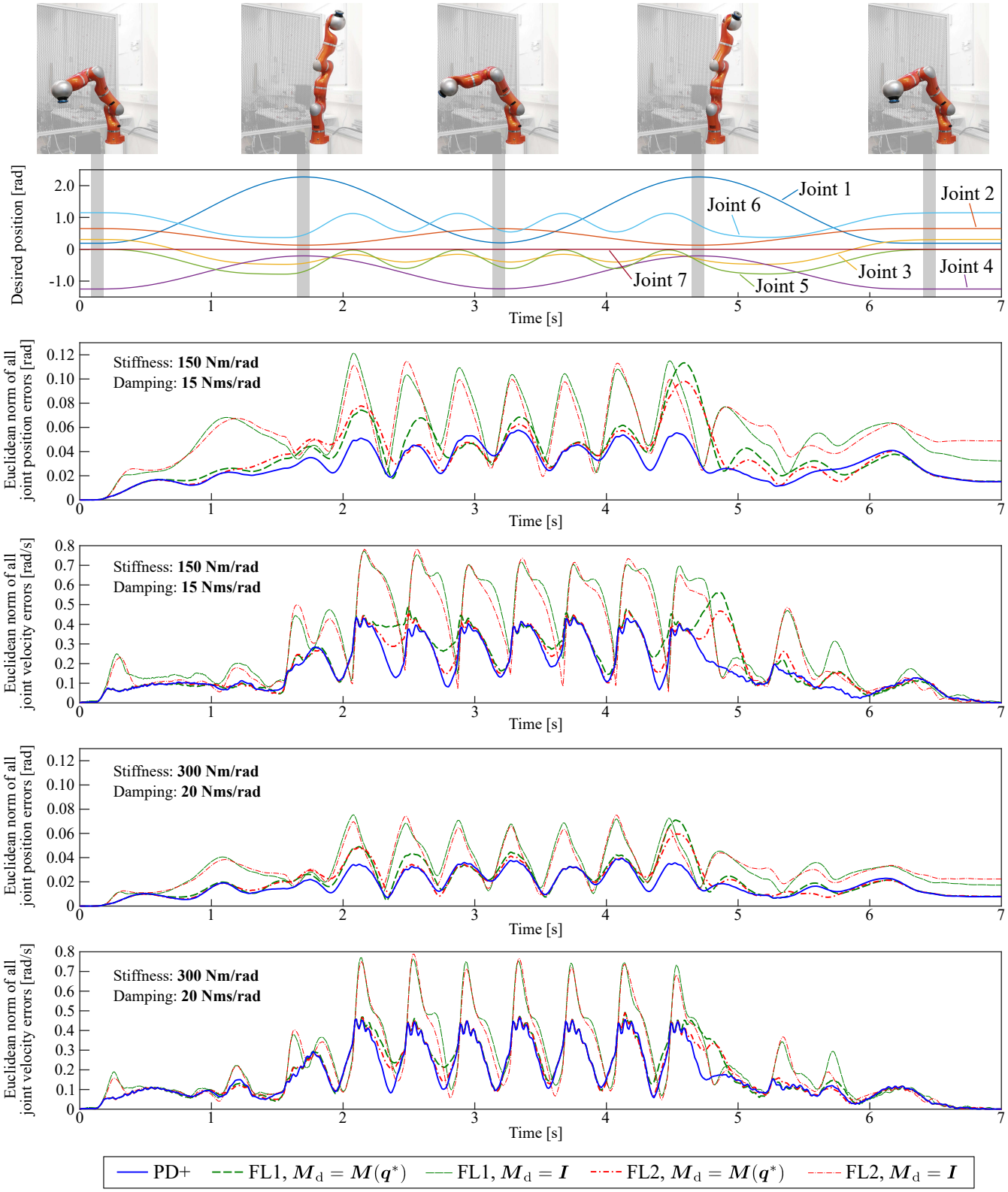

Figure 4: Experiment #1a: Comparison of the control performance in free-motion trajectory tracking. The feedback linearizations FL1 and FL2 are evaluated with $\boldsymbol{M}_\mathrm{d} = \boldsymbol{M}(\boldsymbol{q}^*)$ and $\boldsymbol{M}_\mathrm{d} = \boldsymbol{I}$ each. The joint stiffness and damping values are set to $\boldsymbol{K} = \mathrm{diag}(150, \ldots, 150)$ Nm/rad, $\boldsymbol{D} = \mathrm{diag}(15, \ldots, 15)$ Nms/rad (diagrams 2, 3) and set to $\boldsymbol{K} = \mathrm{diag}(300, \ldots, 300)$ Nm/rad, $\boldsymbol{D} = \mathrm{diag}(20, \ldots, 20)$ Nms/rad (diagrams 4 and 5).

Table 2: Comparison of the theoretical properties of PD+ control and feedback linearization control (FL1 & FL2)

Property	**PD+**	**FL1 (w/ $\boldsymbol{\tau}_{\text{ext}}$ feedback)**	**FL2 (w/o $\boldsymbol{\tau}_{\text{ext}}$ feedback)**
Control feedback variables	$\boldsymbol{e}, \dot{\boldsymbol{e}}$	$\boldsymbol{e}, \dot{\boldsymbol{e}}, \boldsymbol{\tau}_{\text{ext}}$	$\boldsymbol{e}, \dot{\boldsymbol{e}}$
Tuning parameters	$\boldsymbol{K}, \boldsymbol{D}$	$\boldsymbol{K}, \boldsymbol{D}, \boldsymbol{M}_{\text{d}}$; poles and $\boldsymbol{M}_{\text{d}}$ or $\boldsymbol{K}$	poles; $\boldsymbol{M}_{\text{d}}^{-1}\boldsymbol{K}, \boldsymbol{M}_{\text{d}}^{-1}\boldsymbol{D}$
Passivity and stability	Passive, asymptotic	Passive, exponential	Not passive, exponential
Perceived stiffness and inertia	$\boldsymbol{K}$, $\boldsymbol{M}(\boldsymbol{q})$	$\boldsymbol{K}$, $\boldsymbol{M}_{\text{d}}$	$\boldsymbol{M}(\boldsymbol{q})\boldsymbol{M}_{\text{d}}^{-1}\boldsymbol{K}$, $\boldsymbol{M}(\boldsymbol{q})$
Effective control gains for $\boldsymbol{e}, \dot{\boldsymbol{e}}$	$-\boldsymbol{K}, -\boldsymbol{D}$	$-\boldsymbol{M}(\boldsymbol{q})\boldsymbol{M}_{\text{d}}^{-1}\boldsymbol{K}, -\boldsymbol{M}(\boldsymbol{q})\boldsymbol{M}_{\text{d}}^{-1}\boldsymbol{D}$	$-\boldsymbol{M}(\boldsymbol{q})\boldsymbol{M}_{\text{d}}^{-1}\boldsymbol{K}, -\boldsymbol{M}(\boldsymbol{q})\boldsymbol{M}_{\text{d}}^{-1}\boldsymbol{D}$
Effective control gains for $\boldsymbol{\tau}_{\text{ext}}$	-	$\boldsymbol{M}(\boldsymbol{q})\boldsymbol{M}_{\text{d}}^{-1} - \boldsymbol{I}$	-
Influence of $\boldsymbol{\tau}_{\text{nonpar}}$, see (24)	Not altered	Distorted by $\boldsymbol{M}_{\text{d}}\boldsymbol{M}(\boldsymbol{q})^{-1}$	Distorted by $\boldsymbol{M}_{\text{d}}\boldsymbol{M}(\boldsymbol{q})^{-1}$
Influence of $\tilde{\boldsymbol{M}}(\boldsymbol{q})$, see (30)	Depending on $\ddot{\boldsymbol{q}}_{\text{d}}$, not altered	Depending on $\boldsymbol{e}, \dot{\boldsymbol{e}}, \ddot{\boldsymbol{q}}_{\text{d}}, \boldsymbol{\tau}_{\text{ext}}$, distorted by $\boldsymbol{M}_{\text{d}}\boldsymbol{M}(\boldsymbol{q})^{-1}$	Depending on $\boldsymbol{e}, \dot{\boldsymbol{e}}, \ddot{\boldsymbol{q}}_{\text{d}}$, distorted by $\boldsymbol{M}_{\text{d}}\boldsymbol{M}(\boldsymbol{q})^{-1}$
Influence of $\tilde{\boldsymbol{C}}(\boldsymbol{q}, \dot{\boldsymbol{q}})$, see (31)	Depending on $\dot{\boldsymbol{q}}_{\text{d}}$, not altered	Depending on $\dot{\boldsymbol{q}}$, distorted by $\boldsymbol{M}_{\text{d}}\boldsymbol{M}(\boldsymbol{q})^{-1}$	Depending on $\dot{\boldsymbol{q}}$, distorted by $\boldsymbol{M}_{\text{d}}\boldsymbol{M}(\boldsymbol{q})^{-1}$
Influence of $\tilde{\boldsymbol{g}}(\boldsymbol{q})$, see (32)	Not altered	Distorted by $\boldsymbol{M}_{\text{d}}\boldsymbol{M}(\boldsymbol{q})^{-1}$	Distorted by $\boldsymbol{M}_{\text{d}}\boldsymbol{M}(\boldsymbol{q})^{-1}$

Table 3: Overview of the experiments

Exp.	**Description**
#1a	Tracking, fast motion, setting of stiffness/damping/(inertia)
#1b	Tracking, moderate motion, instability with FL1 and FL2
#1c	Tracking, moderate motion, instability with PD+
#1d	Tracking, fast motion, maximum control gains
#1e	Step response, moderate control gains
#2a	Slow interaction, application of (virtual) external torque
#2b	Slow interaction, physical contact
#2c	Perceived inertia, application of (virtual) external torque

Table 4: Minimum and maximum scaling coefficients in the feedback control gains in FL1/FL2 during experiment #1a

Scaling of control gains via eigenvalues of $\boldsymbol{M}(\boldsymbol{q})\boldsymbol{M}_{\text{d}}^{-1}$, (5) and (7)	$\boldsymbol{M}_{\text{d}} = \boldsymbol{M}(\boldsymbol{q}^*)$	$\boldsymbol{M}_{\text{d}} = \boldsymbol{I}$
Maximum reduction	0.22 (red. by 78%)	0.09 (red. by 91%)
Maximum amplification	1.43 (incr. by 43%)	4.41 (incr. by 341%)

4.1. Experiment #1a (tracking, fast motion, setting of stiffness/damping/(inertia))

In experiment #1a, highly dynamic desired joint-space trajectories are executed as shown in Fig. 4 (top diagram), yielding maximum velocities at the end-effector of up to 1.52 m/s. The implementation covers the PD+ and both considered types of feedback linearizations. For both FL1 and FL2, two desired inertia parametrizations are used: $\boldsymbol{M}_{\text{d}}$ is set to $\boldsymbol{M}(\boldsymbol{q}^*)$ (see Fig. 2, left picture) and $\boldsymbol{I}$. While the first inertia distribution is certainly closer to the natural one, the identity matrix is often used in robotics and especially in the field of inverse dynamics [26, 50, 30]. Initially, the stiffness and damping values are set to $\boldsymbol{K} = \text{diag}(150, \ldots, 150)$ Nm/rad, $\boldsymbol{D} = \text{diag}(15, \ldots, 15)$ Nms/rad. The results are depicted in the diagrams 2 and 3 of Fig. 4. Therein, the Euclidean norms of the joint position and velocity errors are plotted, respectively. One can observe that the PD+ features the smallest maximum errors and performs slightly better than FL1 and FL2 for $\boldsymbol{M}_{\text{d}} = \boldsymbol{M}(\boldsymbol{q}^*)$. However, the desired inertia of $\boldsymbol{M}_{\text{d}} = \boldsymbol{I}$ leads to significantly larger errors in the positions and velocities which reflects the theoretical findings obtained in Section 3. Due to deviations between the natural, configuration-dependent inertia $\boldsymbol{M}(\boldsymbol{q})$ and the desired inertia $\boldsymbol{M}_{\text{d}}$, the feedback control gains for stiffness and damping are scaled through pre-multiplication by $\boldsymbol{M}(\boldsymbol{q})\boldsymbol{M}_{\text{d}}^{-1}$, see (5) and (7). In Table 4, the minimum and maximum eigenvalues of $\boldsymbol{M}(\boldsymbol{q})\boldsymbol{M}_{\text{d}}^{-1}$ during experiment #1a are listed to get an insight into this scaling action. For $\boldsymbol{M}_{\text{d}} = \boldsymbol{M}(\boldsymbol{q}^*)$, the scaling ranges from a reduction by 78 % up to an increase by 43 %. In other words, depending on the current configuration $\boldsymbol{q}$, the nominal feedback gains for $\boldsymbol{e}$ and $\dot{\boldsymbol{e}}$ may be reduced or increased. Selecting $\boldsymbol{M}_{\text{d}} = \boldsymbol{I}$ can lead to a potentially even more conservative but also more aggressive control action. In some joint configurations, the feedback gains for position and velocity errors are reduced by 91 %, while the gains are increased by up to 341 % in other cases. Depending on the selected nominal values for stiffness and damping, such a scaling may cause instability in practice as will be shown later. A similar behavior as the one in the diagrams 2 and 3 can be obtained for higher impedance specifications, namely $\boldsymbol{K} = \text{diag}(300, \ldots, 300)$ Nm/rad and $\boldsymbol{D} = \text{diag}(20, \ldots, 20)$ Nms/rad. The results are depicted the diagrams 4 and 5 of Fig. 4. One can see that the errors in all approaches are reduced but the relative differences between the controllers remain. That similarity can also be observed in Fig. 5 where the root mean square (RMS) and maximum values of all error norms in Fig. 4 are condensed. As expected, higher values for $\boldsymbol{K}$ (with proper choice of $\boldsymbol{D}$) tendentially yield smaller tracking errors. Yet, one can summarize that the PD+ features the

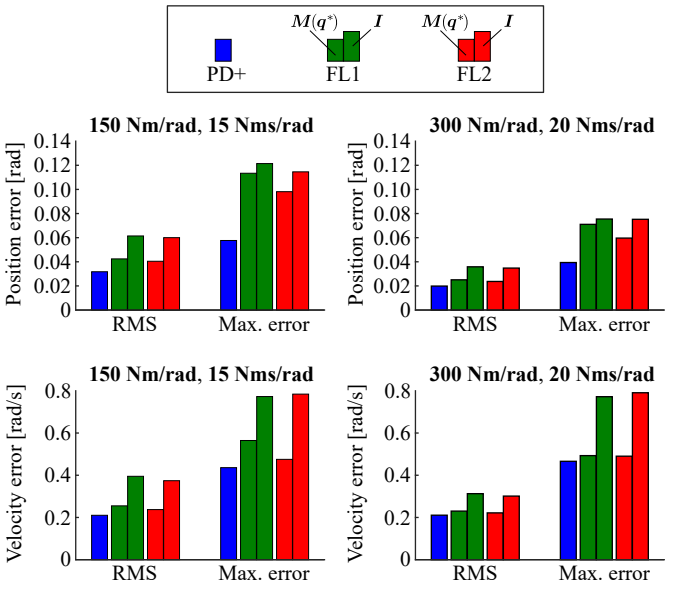

Figure 5: Exp. #1a: Root mean square (RMS) and maximum values of all error norms in Fig. 4 for all transients. The left bars in FL1 and FL2 describe the case for $\boldsymbol{M}_\mathrm{d} = \boldsymbol{M}(\boldsymbol{q}^*)$, whereas the right bars correspond to $\boldsymbol{M}_\mathrm{d} = \boldsymbol{I}$.

best performance in all cases, and $\boldsymbol{M}_\mathrm{d} = \boldsymbol{M}(\boldsymbol{q}^*)$ is superior to $\boldsymbol{M}_\mathrm{d} = \boldsymbol{I}$ in both FL1 and FL2. Nevertheless, it must be noted that by choosing a specific $\boldsymbol{M}_\mathrm{d}$ to ensure large but feasible eigenvalues of $\boldsymbol{M}(\boldsymbol{q})\boldsymbol{M}_\mathrm{d}^{-1}$, FL1 and FL2 can potentially feature an even higher tracking performance than PD+ control. However, such a case can be intuitively interpreted as an increased effective value of $\boldsymbol{K}$ and $\boldsymbol{D}$ for PD+ control. Therefore, an obvious and simple alternative for FL1/FL2 is to directly increase $\boldsymbol{K}$ and $\boldsymbol{D}$ instead of achieving this effect by shaping $\boldsymbol{M}_\mathrm{d}$.

4.2. Experiment #1b (tracking, moderate motion, instability with FL1/FL2)

In experiment #1b the stability problems of the feedback linearizations are experimentally verified which have been identified in Section 3.6 and originate from the potentially problematic scaling of the feedback gains for $\boldsymbol{e}$ and $\dot{\boldsymbol{e}}$ through the coefficient $\boldsymbol{M}(\boldsymbol{q})\boldsymbol{M}_\mathrm{d}^{-1}$. Instead of the forward-backward-forward-backward motion from experiment #1a, only one forward-backward motion is executed as desired joint-space trajectory in experiment #1b. Moreover, this reference trajectory is slowed down for the sake of safety. The control gains are modified as follows:

$$\boldsymbol{K} = \mathrm{diag}(1500, 1500, 150, 150, 150, 150, 150)\,\mathrm{Nm/rad}\ ,$$
$$\boldsymbol{D} = \mathrm{diag}(90, 90, 15, 15, 7, 7, 7)\,\mathrm{Nms/rad}\ .$$

Thus, the stiffness and damping values for the largest joints (1 and 2) are increased, where the values for the other joints are kept constant or get reduced. In the following, the behaviors in FL1 and FL2 with the common choice $\boldsymbol{M}_\mathrm{d} = \boldsymbol{I}$ are investigated. As a basis for the comparison, the PD+ is also considered with the same parameters for $\boldsymbol{K}$ and $\boldsymbol{D}$.

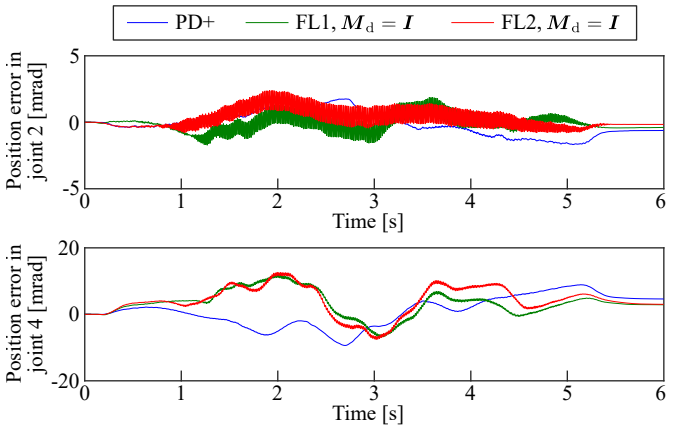

Figure 6: Exp. #1b: Instability with feedback linearizations (FL1, FL2) due to configuration-dependent scaling of the feedback gains, illustrated through the errors in the joint positions

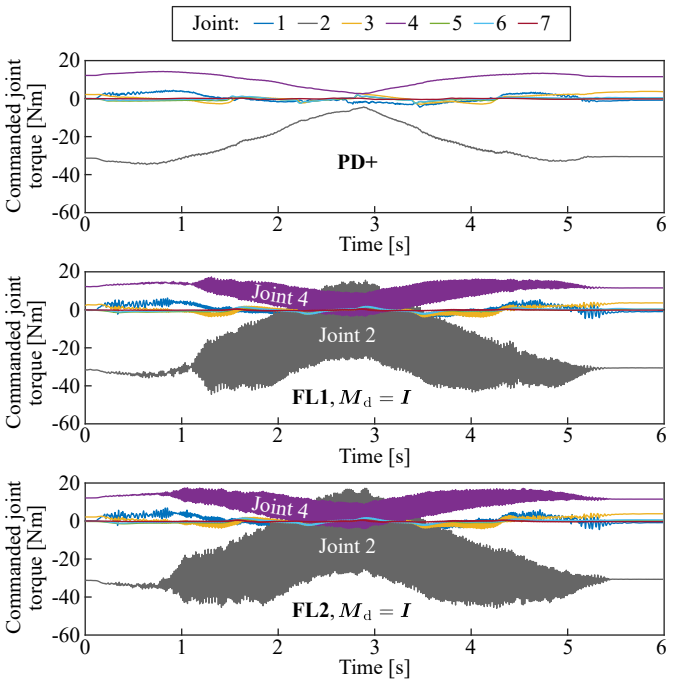

Figure 7: Exp. #1b: Instability with feedback linearizations (FL1, FL2) due to configuration-dependent scaling of the feedback gains, illustrated through the commanded joint torques

In Fig. 6, the position errors in the joints 2 and 4 are depicted because they indicate problems in terms of stability in case of FL1 and FL2 control. While the PD+ yields a stiff but stable behavior, both feedback linearizations lead to significant oscillations during the transient, especially in joint 2.[7] These vibrations can also be seen in the commanded joint torques, see Fig. 7. While the PD+ shows proper torques in all joints, high-frequency oscillations occur in both FL1 and FL2. The reason for these problems can be found in the right column of Table 4,

[7]The other five joint position errors (1, 3, 5, 6, and 7) are not depicted here since no noteworthy oscillations occur in these signals.

which can also be consulted here due to the comparable desired joint-space trajectories. The maximum eigenvalue of $\boldsymbol{M}(\boldsymbol{q})\boldsymbol{M}_{\mathrm{d}}^{-1}$ reaches 4.41 at about 2.5 s, meaning that in one specific direction, the feedback gain is increased by about 341 %. Consulting the respective eigenvector reveals the distribution

$$(0.03, \mathbf{0.94}, 0.03, \mathbf{\text{-}0.33}, 0.01, 0.02, -0.01)^T \ .$$

One can clearly see that the dominating parts relate to joint 2 (0.94) and joint 4 (-0.33). For that reason the largest oscillations appear in joint 2, followed by joint 4, as also observed in Fig. 7. These vibrations are not due to torque saturations but limitations in the torque bandwidth. Interestingly, the aggressive scaling of the feedback gains leads to the opposite effect in other directions at the same time. Simultaneously, that is, at about 2.5 s, the instantaneous minimum eigenvalue of $\boldsymbol{M}(\boldsymbol{q})\boldsymbol{M}_{\mathrm{d}}^{-1}$ is about 0.09 with the corresponding eigenvector

$$(0.01, 0, 0.1, -0.03, \mathbf{\text{-}0.76}, -0.02, \mathbf{0.64})^T \ .$$

Herein the joints 5 and 7 dominate. As a result, the feedback control gains in this direction are significantly reduced. While that does not necessarily jeopardize the stability of the closed loop, it can lead to large deviations between desired and actual behavior in practice.

4.3. Experiment #1c (tracking, moderate motion, instability with PD+)

In experiment #1c the stability problems of the PD+ controller (Section 3.1) are experimentally verified. The desired trajectories from experiment #1b are executed. One of the main advantages of the feedback linearization is the possibility to assign constant, desired closed-loop poles. These are set to -25 in all seven joints with $\boldsymbol{M}_{\mathrm{d}} = \boldsymbol{I}$ in the following. Such eigenvalues represent a practical choice for the considered type of lightweight robots [44].

The top diagram of Fig. 8 shows the results of both feedback linearizations FL1/FL2. Moreover, the results for the PD+ controlled robot are shown wherein the constant values for $\boldsymbol{K}$ and $\boldsymbol{D}$, taken from the feedback linearizations, are directly used. The constant desired closed-loop poles cannot be realized in case of the PD+ by definition since the required constant inertia $\boldsymbol{M}_{\mathrm{d}}$ is not implemented but the variable, natural one $\boldsymbol{M}(\boldsymbol{q})$ is conserved. One can see that the PD+ controlled system shows oscillations in the Euclidean norm of all joint position errors. These vibrations are primarily due to the fact that the effective feedback gains in the joints close to the end-effector are too high for the respective joint torque controllers. As depicted in the second diagram, all effective gains are set to 625 Nm/rad, exceeding the limits of some of the joints. That leads to at least one aggressive local pole that attains values of about -544 as can be observed in the third diagram.[8] The eigenvectors which correspond to these aggressive local PD+ poles are primarily related to the mentioned joints close to the end-effector, which have to accelerate significantly lower inertias than the first joints of the manipulator. These joints can be directly identified when investigating the resulting commanded joint torques (fourth diagram), indicating that the critical signals relate to the fifth and sixth joint.

[8] For PD+ control the closed-loop poles are locally approximated via the quasi-static, interaction-free version of (4) in 25 ms steps, i. e., only based on $\boldsymbol{M}(\boldsymbol{q}), \boldsymbol{D}, \boldsymbol{K}$, with $\boldsymbol{C}(\boldsymbol{q}, \boldsymbol{0}) = \boldsymbol{0}$ and $\boldsymbol{\tau}_{\mathrm{ext}} = \boldsymbol{0}$.

Table 5: Maximum controller gains (experiment #1d), empirically chosen, with $\boldsymbol{M}_{\mathrm{d}} = \boldsymbol{I}$ for FL1/FL2

Joint number	**PD+** (stiffness, damping†)	**FL1/FL2** (stiffness, damping ratio, poles)
1	1500 Nm/rad, 0.5-0.7	1500 Nm/rad, 0.71, -27.5±27.3i
2	1500 Nm/rad, 0.5-0.7	900 Nm/rad, 0.50, -15.0±26.0i
3	1000 Nm/rad, 0.5-0.7	1225 Nm/rad, 0.57, -20.0±28.7i
4	1000 Nm/rad, 0.5-0.7	900 Nm/rad, 0.50, -15.0±26.0i
5	300 Nm/rad, 0.5-0.7	1225 Nm/rad, 0.71, -25.0±24.5i
6	300 Nm/rad, 0.5-0.7	1225 Nm/rad, 0.71, -25.0±24.5i
7	300 Nm/rad, 0.5-0.7	1225 Nm/rad, 0.71, -25.0±24.5i

† The damping refers to the damping ratios in the modal directions of the coupled dynamics. That includes the damping ratios: 3×0.5, 4×0.7.

In case of FL1 and FL2, the constant closed-loop poles lead to variable and largely different effective feedback gains between 56 Nm/rad and 2753 Nm/rad. Even the largest gain does not jeopardize stability since the corresponding eigenvector mainly relates to the first joints of the manipulator, which can handle such high values better. The latter can also be observed in the fifth and sixth diagram of Fig. 8 that features proper joint torque commands. This experiment demonstrates one of the major benefits of FL1/FL2 control. The feedback linearization implicitly chooses adequate effective gains in the joints by incorporating the current inertia distribution to implement desired closed-loop poles.

4.4. Experiment #1d (tracking, fast motion, maximum control gains)

While both experiments #1b and #1c highlighted the occurrence of destabilization due to inappropriate gain design, a comparison of the individually best tracking performances of the investigated methods is still missing. For the following experiment #1d, the controller gains for PD+ and FL1/FL2 control have been chosen by their individually most appropriate gain selection procedure. In Table 5, these respective values are listed. In case of the PD+, the stiffness values have been empirically chosen according to the capabilities of the hardware (motors in the joints, gear ratios, inertias to accelerate). Therefore, the first joints can handle larger stiffness values, whereas the gains in the last joints are significantly smaller. The damping has been implemented based on the double diagonalization method [51] which realizes damping ratios in the modal

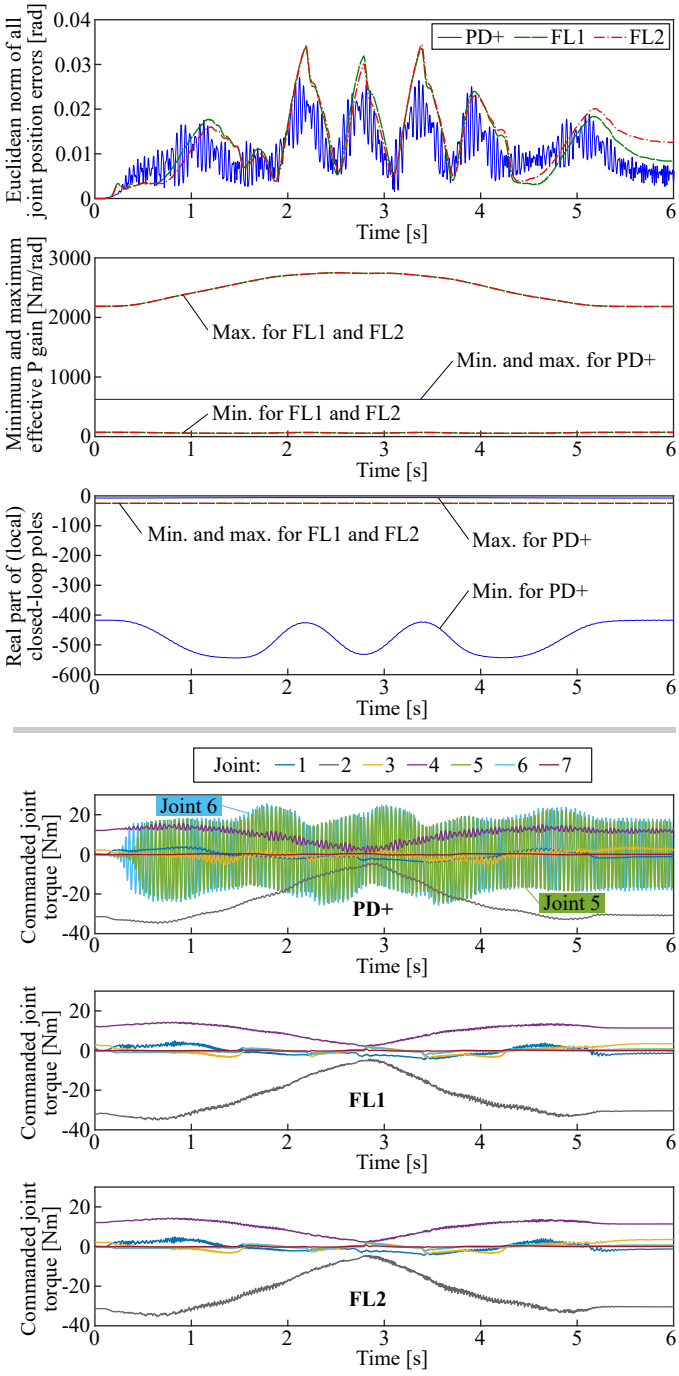

Figure 8: Exp. #1c: Instability with PD+ due to direct adoption of $\boldsymbol{K}, \boldsymbol{D}$ from FL1/FL2. The feedback linearizations have been parametrized with $\boldsymbol{M}_\mathrm{d} = \boldsymbol{I}$ and all closed-loop poles set to -25. The approximated (local) closed-loop poles computed and displayed in 25 ms steps are shown in the third plots. The commanded joint torques for PD+ control indicate instability, particularly due to the signals in the joints 5 and 6.

directions of the nonlinear dynamics[9]. It has to be noted that these damping ratios (3×0.5, 4×0.7) do not directly correspond to the separate joint motions due to the natural coupling in the inertia matrix. In case of FL1/FL2 control, the closed-loop poles of the decoupled dynamics have been empirically specified and $\boldsymbol{M}_\mathrm{d} = \boldsymbol{I}$ has been set. The corresponding damping ratios have been chosen such that the poles lie as far away from the real axis as possible without inducing vibrations. The resulting stiffness values and damping ratios of (6) and (8) are listed in Table 5 and supplemented by the locations of the poles. The same, highly dynamic desired joint-space trajectory as in experiment #1a (Fig. 4, top diagram) is applied.

In Fig. 9 all position errors are compared. The PD+ controller appears to perform best in most of the joints. Note that in the first joint, the maximum velocities are reached four times, at about $\pm 2.09\,\mathrm{rad/s}$ at $t \approx 1, 2.5, 4, 5.5\,\mathrm{s}$, marked by the shaded areas in the top diagram of Fig. 9.[10] That results in the corresponding position errors in joint 1. One can analyze the influence on the remaining six joint position errors in the diagrams 2–7 of Fig. 9. While the errors in the first joint do not lead to noticeable actions and effects on the other joints with the PD+, both FL1 and FL2 show direct reactions. Especially in the joints 3 and 4, one can identify errors in the joint positions which are induced by the errors in the first joint. This is a direct consequence of the cross-couplings of the feedback of the signals $\boldsymbol{e}, \dot{\boldsymbol{e}}$ in the control laws (5) and (7) through the coefficient $\boldsymbol{M}(\boldsymbol{q})\boldsymbol{M}_\mathrm{d}^{-1}$. Although the theory demands a nominal decoupling for the trajectory tracking case, the FL1/FL2 control laws lead to dynamic couplings in the presence of unmodeled effects in practice (here: velocity saturations).

A more concise overview of the tracking performance is provided in Fig. 10, wherein the Euclidean norms of all joint position and velocity errors are plotted, respectively. While the differences in the joint velocity errors are rather small, the tracking performance in terms of the position errors shows a better behavior with PD+ control. In the third plot of Fig. 10, the control input power $\dot{\boldsymbol{q}}^T\boldsymbol{\tau}$ is depicted. One can observe that most of the time the power exchanges for PD+ and FL1/FL2 are almost identical. However, during the times of joint velocity saturation in joint 1 (Fig. 10, shaded areas in top diagram at $t \approx 1, 2.5, 4, 5.5\,\mathrm{s}$), the control action in case of FL1/FL2 requires more control input power and still yields an inferior tracking performance. The bottom diagram in Fig. 10 shows the minimum and maximum real parts of the closed-loop poles for FL1/FL2 and PD+, respectively. Interestingly, at least one PD+ pole has a real part of about -45. However, it has to be noted that the eigenvectors corresponding to the respective poles are different for FL1/FL2 and PD+. Furthermore, the PD+ poles are only local approximations indicating a tendency, but they do not accurately represent the nonlinear dynamics.

The control input power from the third diagram in Fig. 10 is divided in two components in Fig. 11, namely

[9] computed for the quasi-static, interaction-free version of the equations of motion ($\boldsymbol{C}(\boldsymbol{q}, \boldsymbol{0}) = \boldsymbol{0}$, $\boldsymbol{\tau}_\mathrm{ext} = \boldsymbol{0}$) and updated with 1 kHz.

[10] The maximum velocities are due to back electromotive forces. To avoid reaching these limits, one can use conservative values for the trajectory design, for example $\pm\{1.9, 1.9, 2.2, 2.2, 3.6, 3.2, 3.2\}$ rad/s.

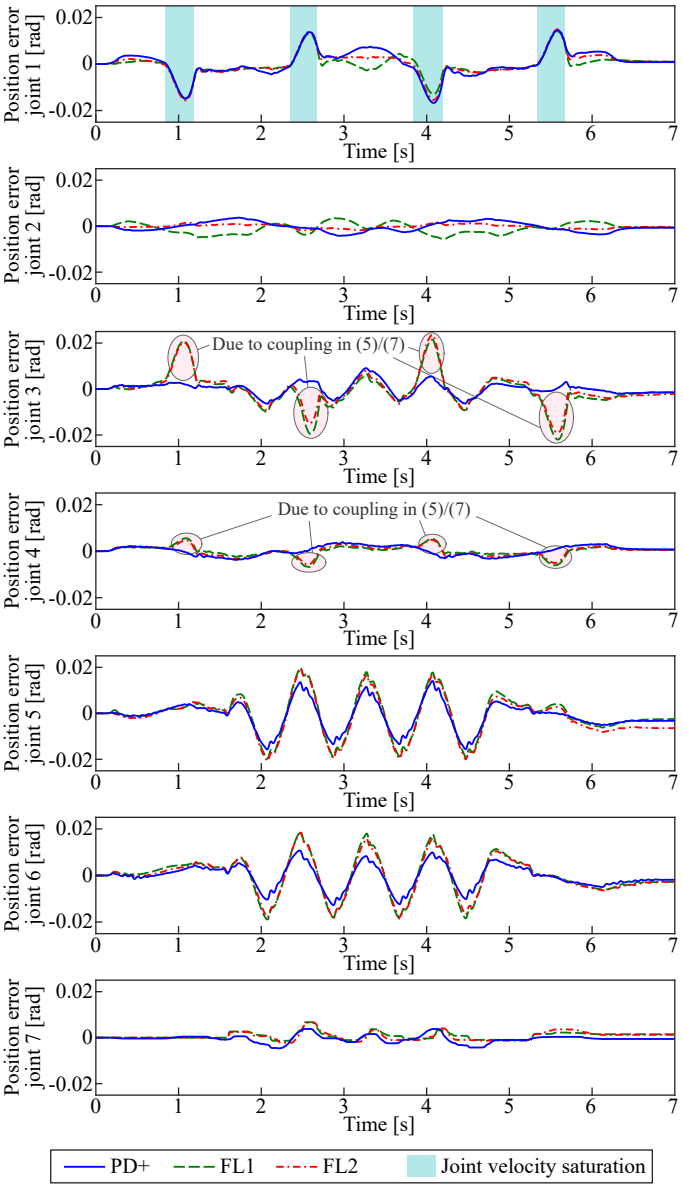

Figure 9: Exp. #1d (tracking comparison): The maximum control gains have been empirically chosen for PD+ and FL1/FL2. The position errors in all joints are depicted.

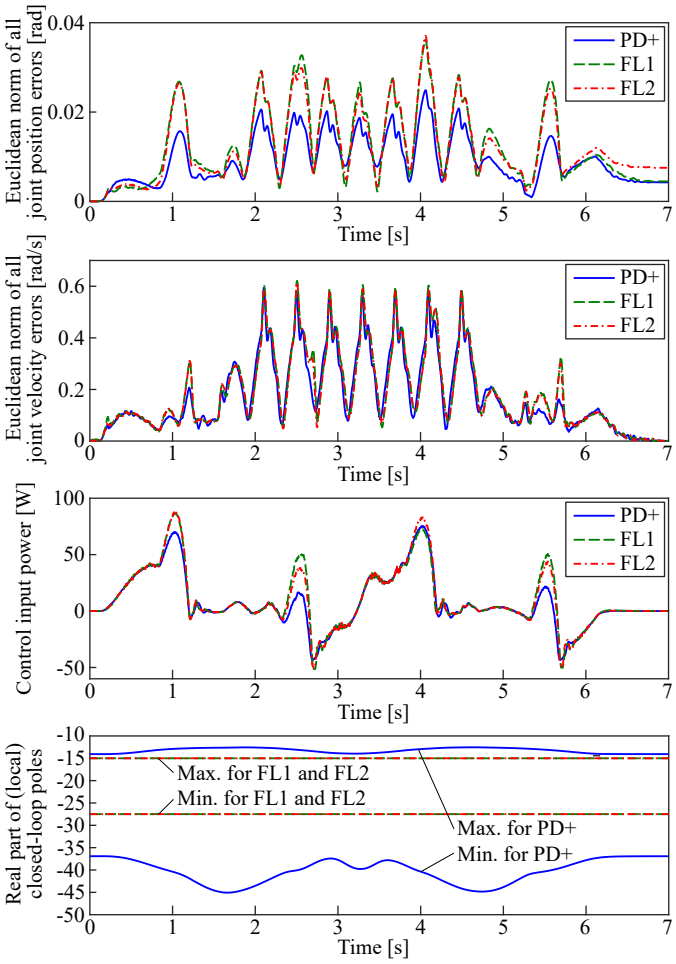

Figure 10: Exp. #1d (tracking comparison): The maximum control gains have been empirically chosen for PD+ and FL1/FL2, and the Euclidean error norms in the positions and velocities are compared. The control input power in the third diagram is given by $\dot{\boldsymbol{q}}^T\boldsymbol{\tau}$. The bottom diagram shows the (approximated, local) closed-loop poles computed and displayed in 25 ms steps.

one related to the compensation/'+' action and one related to the pure PD control part.[11]. When comparing PD+ and FL2 one can see that the compensation action in FL2 and the '+' part in the PD+ are almost identical. Only FL1 reveals deviations which can be traced back to the feedback of $\boldsymbol{\tau}_{\text{ext}}$. Note that the whole motion in experiment #1d is performed in free motion. Therefore, $\boldsymbol{\tau}_{\text{ext}}$ should ideally be zero. Consequently, the following conclusions are based on the sole comparison between PD+ and FL2.[12] The main differences are due to the PD parts (Fig. 11, bottom diagram), that is, the feedback of the position and velocity errors, respectively. Therefore, one can conclude that the PD control components in (3) and (7) are primarily responsible for the differences in the tracking performance and the control input powers. Moreover, the bottom diagram in Fig. 11 confirms the justification presented above that the cross-coupling via $\boldsymbol{M}(\boldsymbol{q})\boldsymbol{M}_{\text{d}}^{-1}$ in the FL2 control law leads to the deterioration and the higher power consumption. Although FL2 should be theoretically superior, the desired dynamic decoupling of the closed-loop dynamics (8) for $\boldsymbol{\tau}_{\text{ext}} = \boldsymbol{0}$ cannot be achieved to a sufficient degree. Lastly, Figure 12 shows the commanded torques for three exemplary joints with identical, larger, and smaller joint stiffnesses of PD+ and FL1/FL2 control. While a large joint stiffness in the PD+ controller tendentially leads to increased control actions in

[11] The feedback of $\boldsymbol{\tau}_{\text{ext}}$ in FL1 is contained in the compensation action to obtain an isolated signal for the PD part (related to the feedback of $\boldsymbol{e}, \dot{\boldsymbol{e}}$) in the bottom diagram of Fig. 11.

[12] In practice, the erroneous compensation of $\boldsymbol{\tau}_{\text{ext}}$ in FL1 is counterbalanced by control actions in the PD component to achieve comparable tracking performance as FL2 during free motion, cf. Fig. 10 (top plot).

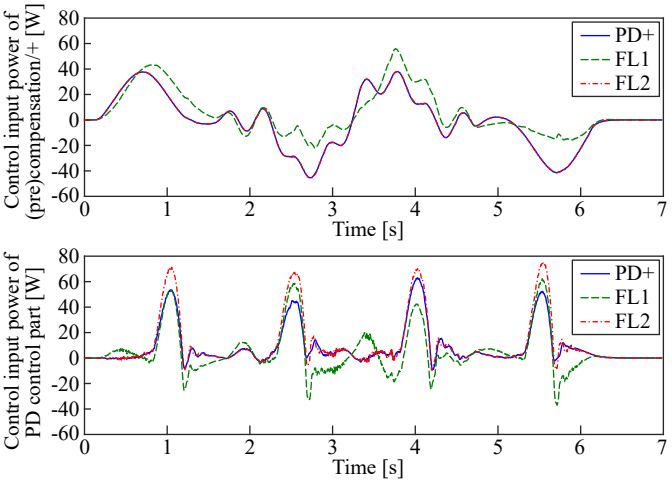

Figure 11: Exp. #1d (tracking comparison): The control input power $\dot{\boldsymbol{q}}^T\boldsymbol{\tau}$ is divided in two components.

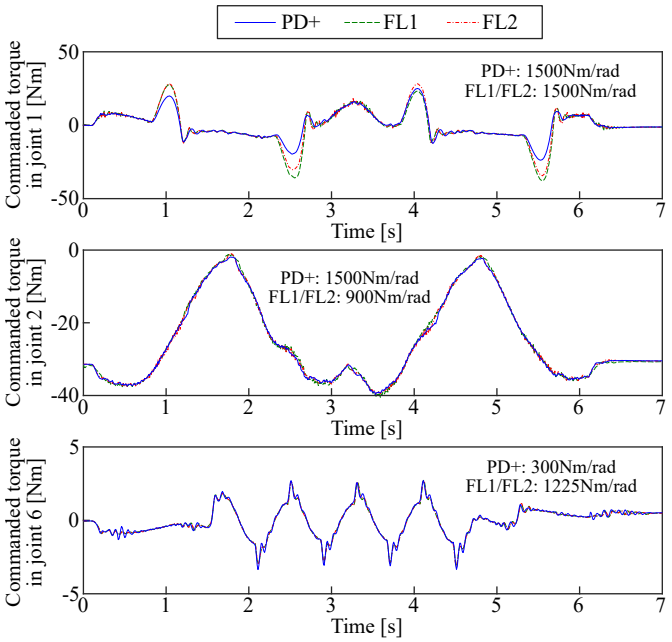

Figure 12: Exp. #1d (tracking comparison): The commanded torques in three exemplary joints are plotted. In joint 1 the PD+ stiffness is identical to the one of FL1/FL2, in joint 2 it is larger, and in joint 6 it is smaller.

this very joint (cf. experiment #1c), that effect does not apply to FL1/FL2 as can be observed in Fig. 12 (bottom diagram). That is again due to the scaling and inter-joint cross-couplings of the feedback control gains via the coefficient $\boldsymbol{M}(\boldsymbol{q})\boldsymbol{M}_{\mathrm{d}}^{-1}$ in FL1/FL2, as discussed in Section 3.6. Therefore, a comparatively large stiffness of 1225 Nm/rad as present in the last joint (Fig. 12, bottom plots) does not necessarily result in a severe control action there.

4.5. Experiment #1e (step response, moderate control gains)

In addition to the trajectory tracking scenarios in the previous experiments, step responses are applied in experiment #1e to investigate the quality of the dynamic decoupling achieved by FL1/FL2. The controller gains are shown in Table 6 and have been chosen smaller than in experiment #1d so that the commanded torques are feasible after the steps without reaching the torque limits. In FL1 and FL2, the desired inertia is set to $\boldsymbol{M}_{\mathrm{d}} = \boldsymbol{I}$. After specification of the poles in both feedback linearization approaches (right column in Table 6), the gains for PD+ (left column) have been determined in a way such that the commanded torques in the joints of the steps are similarly high. The initial configuration for the experiment is again described by $\boldsymbol{M}(\boldsymbol{q}^*)$, i. e., the starting configuration in Fig. 4. The three applied steps are shown in the top diagram of Fig. 13 and cover the following scenarios to provide a fair comparison. In joint 1, the natural inertia in the initial configuration $\boldsymbol{M}(\boldsymbol{q}^*)$ is larger than the one specified for FL1/FL2 (2.75 vs. 1 kg m^2). In joint 2, the values are similar (0.89 vs. 1 kg m^2), and in joint 5, the natural inertia is smaller (0.15 vs. 1 kg m^2).[13] The diagrams 2–4 in Fig. 13 show the Euclidean norms of all position and velocity errors as well as the overall control input powers. In contrast to the tracking case in the previous experiments, the PD+ leads to larger input powers after the steps. That can be examined more closely on the basis of the individual joint response in Fig. 14. The blue shaded areas illustrate the steps, while the areas shaded in yellow demonstrate the influence in the other joints. Especially after the first step, one can clearly observe a successful decoupling in the joints 3 and 4 with both feedback linearizations. In Fig. 15 one can identify the corresponding joint torque commands that lead to this decoupling action. After the steps, both FL1 and FL2 react faster in the other joints than PD+ control, in order to prevent the naturally induced couplings (mainly due to the couplings in $\boldsymbol{M}(\boldsymbol{q})$) to affect the other joints. This control action in FL1/FL2 leads to reduced control input powers as already shown in the bottom diagram of Fig. 13. Summarized, these step responses show that the diagonalization of the inertia matrix and its corresponding joint

Table 6: Controller gains for experiment #1e, empirically chosen, with $\boldsymbol{M}_{\mathrm{d}} = \boldsymbol{I}$ for FL1/FL2

Joint number	**PD+** (stiffness, damping†)	**FL1/FL2** (stiffness, damping ratio, poles)
1	275 Nm/rad, 1.0	100 Nm/rad, 1.0, -10.0
2	275 Nm/rad, 1.0	100 Nm/rad, 1.0, -10.0
3	100 Nm/rad, 1.0	100 Nm/rad, 1.0, -10.0
4	100 Nm/rad, 1.0	100 Nm/rad, 1.0, -10.0
5	15 Nm/rad, 1.0	100 Nm/rad, 1.0, -10.0
6	15 Nm/rad, 1.0	100 Nm/rad, 1.0, -10.0
7	15 Nm/rad, 1.0	100 Nm/rad, 1.0, -10.0

† The damping refers to the damping ratios in the modal directions of the coupled dynamics.

[13] The (1,1), (3,3), and (5,5) elements of $\boldsymbol{M}(\boldsymbol{q}^*)$ are consulted here.

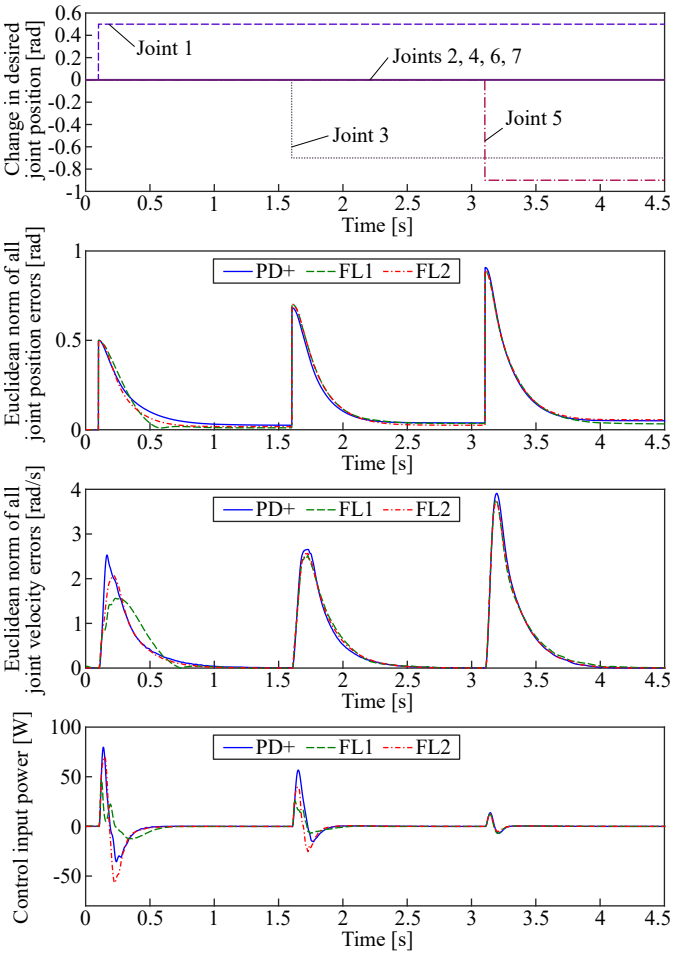

Figure 13: Exp. #1e (step responses): Three steps are applied in the joints 1, 3, and 5. In joint 1, FL1/FL2 scale down the inertia (from 2.75 to 1 kg m^2), in joint 3 it is more or less preserved (from 0.89 to 1 kg m^2), and in joint 5 it is scaled up (from 0.15 to 1 kg m^2).

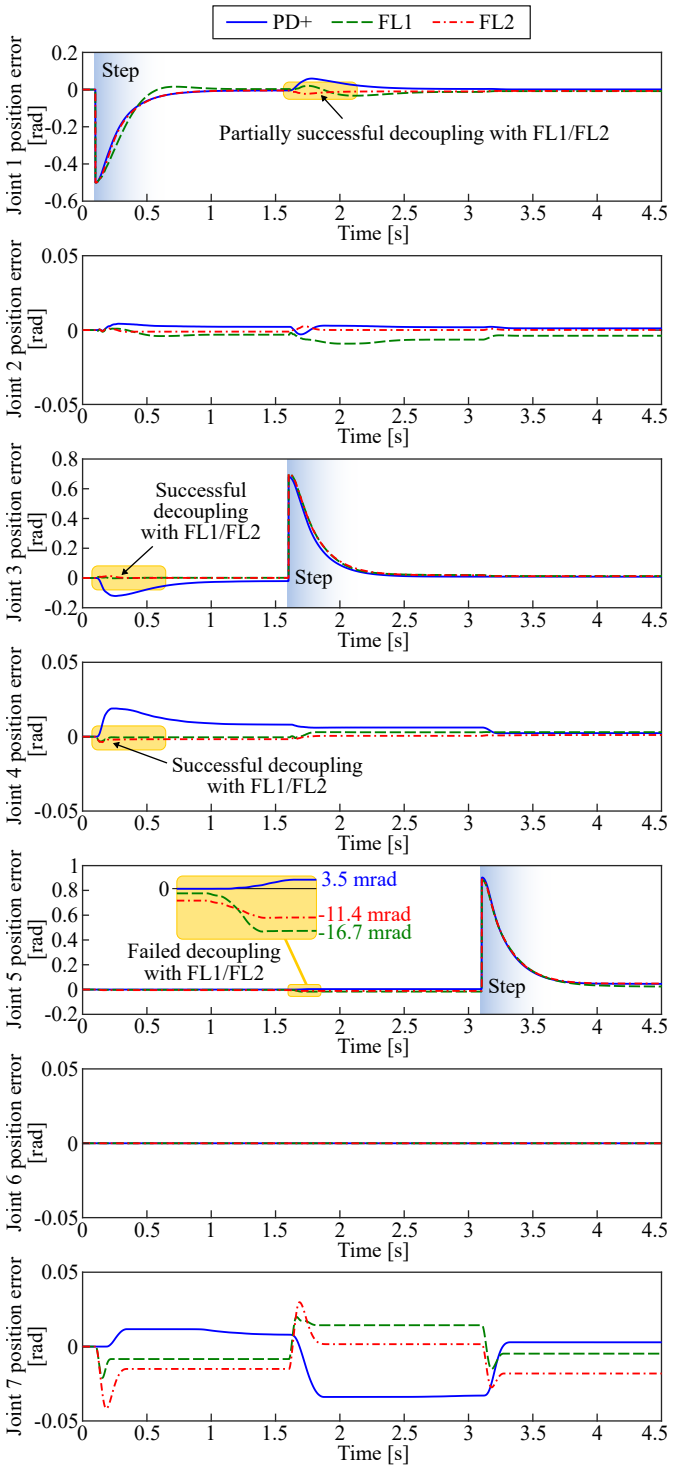

Figure 14: Exp. #1e (step responses): The individual joint responses show that FL1 and FL2 largely succeed in dynamically decoupling the joints. In case of the preservation of the natural inertia (PD+), the application of the steps leads to larger cross-couplings seen as position errors in the other joints.

decoupling can be successfully accomplished by the feedback linearizations. Interestingly, the decoupling appears to be rather effective in step responses (experiment #1e) but it deteriorates the control performance during highly dynamic trajectory tracking (experiment #1d). The reason might be traced back to the fact that the dynamic model (1) is less precise during fast motions where various joints are involved simultaneously.

4.6. Experiment #2a (Slow interaction, application of (virtual) external torque)

In the experiments #2a and #2b the effective contact stiffness is investigated. In experiment #2a a "virtual" external torque is added to the nominal commanded control torque leading to errors in the joint positions, while in experiment #2b a physical contact is enforced and the assessment of the effective stiffness is conducted by relying on the estimated external torque. In both scenarios, the controllers are parametrized as follows: $\boldsymbol{K} = \mathrm{diag}(150, \ldots, 150)$ Nm/rad, $\boldsymbol{D} = \mathrm{diag}(15, \ldots, 15)$ Nms/rad, and $\boldsymbol{M}_\mathrm{d} = \boldsymbol{M}(\boldsymbol{q}^*)$ for FL1 and FL2, analogous to experiment #1a. Figure 16 depicts the results for experiment #2a with a virtual external torque of -15 Nm exerted on joint 1. The disturbance observer output in Fig. 16 (bottom diagram) reflects

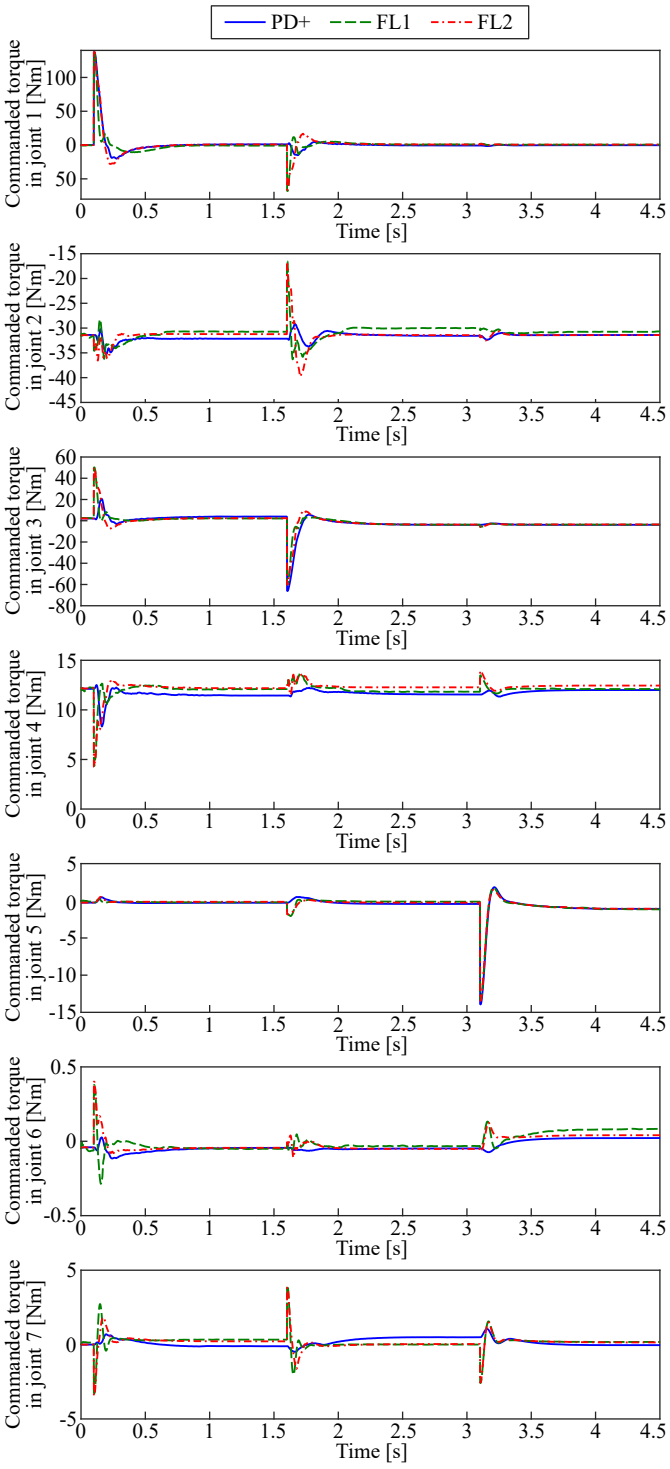

Figure 15: Exp. #1e (step responses): The torque commands shown here correspond to the joint behaviors depicted in Fig. 14.

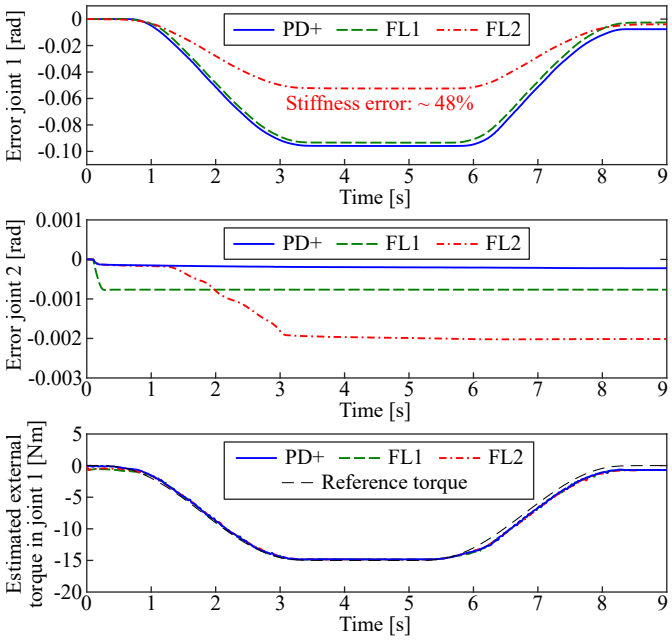

Figure 16: Exp. #2a (contact stiffness): Ideally, the external torque of $-15\,\mathrm{Nm}$ applied on joint 1 and the corresponding stiffness of $150\,\frac{\mathrm{Nm}}{\mathrm{rad}}$ should lead to an error of $-0.1\,\mathrm{rad}$ in joint 1 and zero error in joint 2.

that. The error in the position of joint 1 (top diagram) shows that the PD+ and FL1 adequately implement the desired stiffness of 150 Nm/rad. However, as analyzed in Section 3.3, FL2 control leads to a wrong contact stiffness due to the missing feedback of the estimated external torque. In the considered case, the error in the stiffness amounts to about 48 %. Moreover, small position errors also occur in joint 2. Here, the PD+ performs best but also leads to minor steady-state errors. Nevertheless, both feedback linearizations show larger errors, while the ones in case of FL2 originate from the external torque building up until about 3 s. In fact, that is not surprising as the distorted contact stiffness of $\boldsymbol{M}(\boldsymbol{q})\boldsymbol{M}_\mathrm{d}^{-1}\boldsymbol{K}$ from (22) leads to cross-couplings.

4.7. Experiment #2b (Slow interaction, physical contact)

In experiment #2b the manipulator is driven into contact as illustrated in Fig. 17. As the largest external torque is exerted in joint 1, the evaluation of the effective stiffness is conducted in this joint.[14] In Fig. 18, the position errors in joint 1 and the respective estimated external torques are plotted. The effective contact stiffness is evaluated under static conditions at $t \approx 4\,\mathrm{s}$. Taking into account the desired joint stiffness of 150 Nm/rad, the PD+ and FL1 approaches perform well with ≈147 Nm/rad (≈2% error) and ≈155 Nm/rad (≈3% error), respectively. As expected, FL2 is not able to realize the desired stiffness and shows an effective value of 183 Nm/rad (≈22% error).

In Table 7 the minimum and maximum eigenvalues of $\boldsymbol{M}(\boldsymbol{q})\boldsymbol{M}_\mathrm{d}^{-1}\boldsymbol{K}$ are listed for both experiments #2a and #2b in order to analyze the resulting stiffness for FL2. One can see that, depending on the joint configuration and the particular distribution in $\boldsymbol{e}$, the perceived stiffness can be significantly smaller *or* larger in fact.

[14] Note that the external torques estimated in all other joints are smaller than ±7 Nm, leading to high imprecisions when assessing the corresponding joint-specific stiffnesses during the experiment.

Figure 17: Setup for experiment #2b: After the sixth joint, a physical contact between the robot and its environment is enforced.

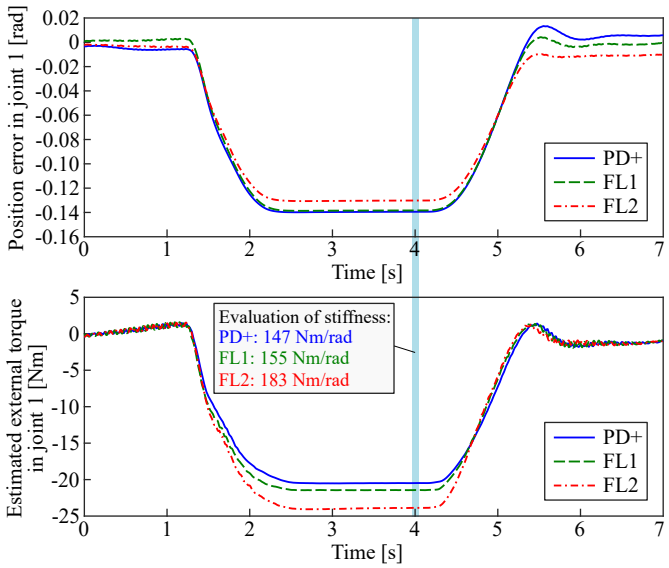

Figure 18: Exp. #2b (contact stiffness): An external force is exerted through physical interaction close to the end-effector. Due to the involvement of all joints, the static joint positions are different in all controllers. The evaluation of the effective stiffness is conducted by means of the first joint at $t \approx 4\,\mathrm{s}$, due to the sufficiently large acting external torque.

Note that both experiments #2a and #2b refer to the external torque observer to assess the achieved contact stiffness. Thus, FL1 is preferred in this assessment by definition as it uses the observer output in (5), in contrast to the PD+ in (3). In practice the observer itself is prone to modeling errors such that the "ground truth" can be rather found in the results of the PD+ control because in quasi-static situations (e. g., at $t \approx 4\,\mathrm{s}$ in both experiments) only the gravity compensation and the stiffness implementation are active, cf. (3). Nevertheless, even then the desired stiffness cannot be accurately achieved in general due to static modeling errors such as static friction or inaccurate gravity compensation. However, these effects are usually minor in practice, e. g., if high-precision joint-torque sensors are used as done in the considered KUKA LWR IV+ or comparable modern torque-controlled lightweight robots.

Table 7: Minimum and maximum stiffness with FL2 during static interaction in the experiments #2a and #2b for the desired/nominal stiffness of 150 Nm/rad

Stiffness via eigenvalues of $\boldsymbol{M}(\boldsymbol{q})\boldsymbol{M}_\mathrm{d}^{-1}\boldsymbol{K}$, (22)	**Exp. #2a**	**Exp. #2b**
Minimum stiffness	79 Nm/rad (error: -47%)	74 Nm/rad (error: -51%)
Maximum stiffness	264 Nm/rad (error: 76%)	268 Nm/rad (error: 79%)

4.8. Experiment #2c (Perceived inertia, application of (virtual) external torque)

In experiment #2c, a virtual external torque is applied analogous to experiment #2a to provide comparable interactions. The focus of this study is to investigate the closed-loop inertial behavior to $\boldsymbol{\tau}_\mathrm{ext}$ out of a static equilibrium (as described in Section 3.3) and during the induced motion. In order to reduce the effects of $\boldsymbol{K}$ and $\boldsymbol{D}$ in the analysis of the inertial behavior, the corresponding gains are set very low in all joints: 10 Nm/rad (stiffness), 2 Nms/rad (damping). Only PD+ and FL1 control are compared in the following since this experiment shall demonstrate the practical consequences of a reduced apparent inertia (FL1) in contrast to the natural one (PD+). The initial configuration of the robot is shown in the right illustration in Fig. 2. An external torque of -5 Nm is commanded to the torque controller in the first and third joint, to represent a horizontally applied interaction force at the end-effector. In case of FL1, $\boldsymbol{M}_\mathrm{d}$ is given by 50 % of the diagonal elements of the natural inertia matrix in the initial configuration, that is, the inertias are actively decoupled and additionally reduced by a factor of 2.

The two top diagrams in Fig. 19 depict the virtual reference torque and the corresponding estimations obtained from the momentum-based disturbance observer. While the estimations for PD+ and FL1 are comparable, the joint motions largely differ, as can be observed in the two bottom diagrams. One can clearly see that the joints start to move earlier and accelerate more in case of FL1 control. That confirms the theoretical claim and advantage that the feedback linearization with feedback of external torques is able to reduce the perceived inertia in practice.

5. Discussion

The entire analysis so far was performed in the joint space of the robot. In general, most of the statements and conclusions can be straightforwardly extended to task-space PD+ [7] and task-space feedback linearization controllers [24], and thus to the comparison between keeping and shaping of the natural inertia in task space. However, due to singularities existing in most task spaces, such as the ones related to the Cartesian coordinates at the end-effectors of manipulators, the globally valid statements made here will then be restricted to their local counterparts. Moreover, the configuration dependencies in the

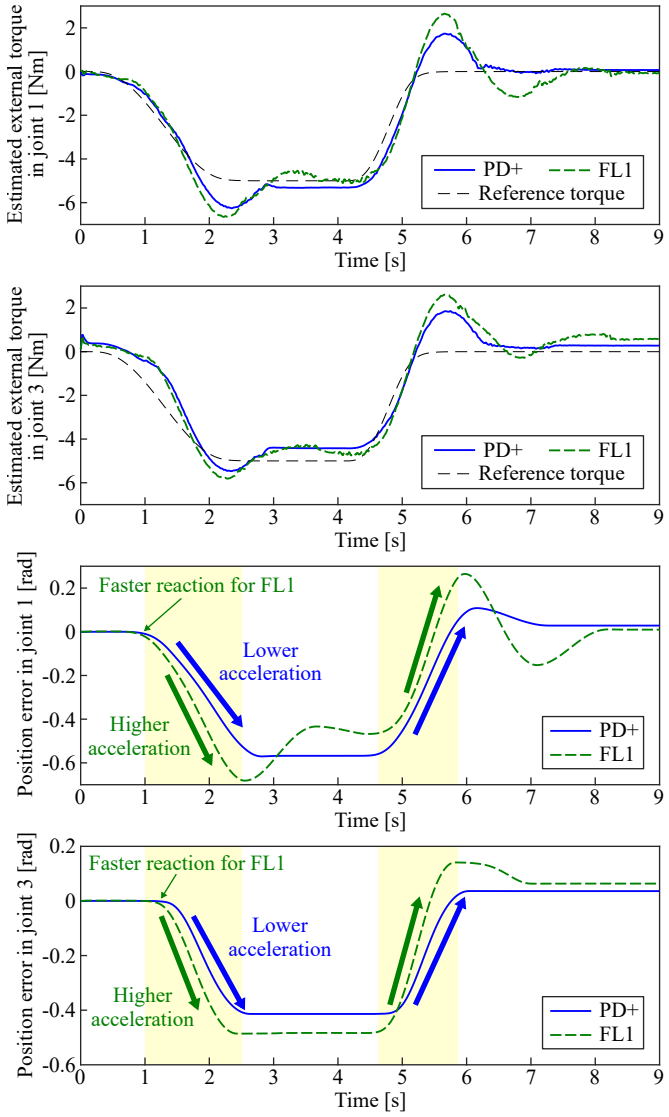

Figure 19: Exp. #2c (inertial response): The reduced apparent/perceived inertia in case of FL1 leads to faster reactions and higher accelerations when external torques are applied.

Jacobian matrices lead to additional couplings that will affect the closed-loop dynamics.

While the experiments have been conducted on one specific robot only, the universality of the conclusions can be extended to a large number of systems. That particularly includes the class of serial-chain, fixed-based, torque-controlled robots. Beyond that, the underlying principles of inertia conservation and shaping also apply to kinematically more complex robots such as humanoids or many free-floating systems.

In case of lacking measurement of $\boldsymbol{\tau}_{\text{ext}}$ required to close the loop in FL1, one can deploy well established and widely used approaches to estimate these signals. For example, by means of momentum-based disturbance observers [49, 47] or various modifications of the latter. Yet, the feedback of $\boldsymbol{\tau}_{\text{ext}}$ (or $\hat{\boldsymbol{\tau}}_{\text{ext}}$, respectively,) inevitably introduces additional complexity in hardware integration/controller-observer design, which can be completely avoided when choosing a control type that does not necessitate its feedback (e. g., PD with feedforward, PD+, FL2). Moreover, the observer itself has limited bandwidth which, in turn, limits the performance of FL1. A practical example has been presented in experiment #2c, where the external torque has not been abruptly applied but continuously increased (see Fig. 19, top diagrams) to remain in the bandwidth of the observer.

Table 8: Summary of the advantages of the preservation of the natural inertia and active inertia shaping

Natural inertia	• No feedback of external torques required • Robust against modeling uncertainties • Interaction behavior intuitive to specify • Close to natural dynamics • Focus on passivity • Predestined for physical interaction
Inertia shaping	• Dynamic decoupling • High design freedom (e. g., pole placement) • Downscaling of the perceived inertia possible • Linear dynamics, tools from linear control applicable • Superior performance for high model accuracy • Predestined for trajectory tracking

While both the keeping and the shaping of the natural dynamics are proven approaches and widely adopted in robotics nowadays, the insights and direct comparisons provided in this article by means of the PD+ and the feedback linearization as representatives, respectively, appear to be crucial for the development of new trajectory tracking and interaction controllers. Since both strategies bring along advantages and disadvantages which affect the theoretical analyses and the practical implementations in different ways, one should be aware of these aspects before making the choice between the preservation of the natural inertia and its active modification by control. Finally, Table 8 serves as a brief summary of the main benefits of both choices.

6. Conclusions

Since many modern robotic systems are required to be both highly accurate and compliant at the same time, an adequate tradeoff between motion tracking performance and physical interaction behavior becomes more and more important. Most model-based controllers can be located between two fundamentally different concepts: the keeping/conservation and the active shaping/modification of the natural inertia. In this article, the consequences and implications of these two border cases have been theoretically and experimentally compared by means of the classical PD+ controller (keeping/conservation) and the classical feedback-linearization/inverse-dynamics/eigenvalue-related design approach (shaping/modification). Practice-oriented analyses have been conducted in terms of gain

tuning procedures, stability and passivity properties, perceived contact stiffness and inertia, influence of modeling uncertainties and imperfect external force feedback, and active scaling of the feedback gains. Several tracking and interaction experiments have been performed to demonstrate the practical relevance of these aspects. Although these two exemplary approaches have been known and established for decades, the understanding of their implications and consequences on physical interaction and trajectory tracking in practice are essential for the development and proper application-driven use of controllers in robotics.

References

[1] R. M. Murray, Z. Li, and S. S. Sastry, *A Mathematical Introduction to Robotic Manipulation*. CRC Press, 1994.

[2] H. K. Khalil, *Nonlinear Systems (Third Edition)*. Prentice Hall, 2002.

[3] N. Hogan, "Impedance Control: An Approach to Manipulation: Part I - Theory, Part II - Implementation, Part III - Applications," *Journal of Dynamic Systems, Measurement, and Control*, vol. 107, pp. 1–24, March 1985.

[4] J. T. Wen and D. S. Bayard, "New class of control laws for robotic manipulators Part 1. Non-adaptive case," *International Journal of Control*, vol. 47, no. 5, pp. 1361–1385, 1988.

[5] R. Kelly, V. Davila Santibáñez, and J. A. Loría Perez, *Control of Robot Manipulators in Joint Space*, ser. Advanced Textbooks in Control and Signal Processing. Springer Science & Business Media, 2005.

[6] B. Paden and R. Panja, "Globally asymptotically stable 'PD+' controller for robot manipulators," *International Journal of Control*, vol. 47, no. 6, pp. 1697–1712, 1988.

[7] C. Ott, *Cartesian Impedance Control of Redundant and Flexible-Joint Robots*, ser. Springer Tracts in Advanced Robotics. Springer Publishing Company, Berlin Heidelberg, 2008, vol. 49.

[8] J.-J. E. Slotine and W. Li, "Adaptive manipulator control: A case study," *IEEE Transactions on Automatic Control*, vol. 33, no. 11, pp. 995–1003, November 1988.

[9] J. Craig, P. Hsu, and S. Sastry, "Adaptive control of mechanical manipulators," in *Proc. of the 1986 IEEE International Conference on Robotics and Automation*, April 1986, pp. 190–195.

[10] R. Middleton and G. Goodwin, "Adaptive computed torque control for rigid link manipulations," *Systems & Control Letters*, vol. 10, no. 1, pp. 9–16, 1988.

[11] M. W. Spong and R. Ortega, "On adaptive inverse dynamics control of rigid robots," *IEEE Transactions on Automatic Control*, vol. 35, no. 1, pp. 92–95, 1990.

[12] S. Fahmi and T. Hulin, "Inertial Properties in Haptic Devices: Non-Linear Inertia Shaping vs. Force Feedforward," *IFAC-PapersOnLine*, vol. 51, no. 22, pp. 79–84, 2018.

[13] M. W. Spong, "Modeling and Control of Elastic Joint Robots," *Journal of Dynamic Systems, Measurement, and Control*, vol. 109, no. 4, pp. 310–319, December 1987.

[14] B. Brogliato, R. Ortega, and R. Lozano, "Global tracking controllers for flexible-joint manipulators: a comparative study," *Automatica*, vol. 31, no. 7, pp. 941–956, 1995.

[15] A. Loría and S. Avila-Becerril, "Output-feedback global tracking control of robot manipulators with flexible joints," in *2014 American Control Conference*, 2014, pp. 4032–4037.

[16] A. Loría, "Observers are unnecessary for output-feedback control of Lagrangian systems," *IEEE Transactions on Automatic Control*, vol. 61, no. 4, pp. 905–920, 2016.

[17] R. Lozano and B. Brogliato, "Adaptive control of robot manipulators with flexible joints," *IEEE Transactions on Automatic Control*, vol. 37, no. 2, pp. 174–181, 1992.

[18] C. Ott, A. Albu-Schäffer, A. Kugi, and G. Hirzinger, "On the Passivity-Based Impedance Control of Flexible Joint Robots," *IEEE Transactions on Robotics*, vol. 24, no. 2, pp. 416–429, April 2008.

[19] M. Iskandar, C. Ott, O. Eiberger, M. Keppler, A. Albu-Schäffer, and A. Dietrich, "Joint-Level Control of the DLR Lightweight Robot SARA," in *Proc. of the 2020 IEEE/RSJ International Conference on Intelligent Robots and Systems*, October 2020.

[20] B. Brogliato, R. Lozano, B. Maschke, and O. Egeland, *Dissipative Systems Analysis and Control: Theory and Applications*, 3rd ed. Springer International Publishing, 2020.

[21] A. Giusti, J. Malzahn, N. G. Tsagarakis, and M. Althoff, "Combined inverse-dynamics/passivity-based control for robots with elastic joints," in *2017 IEEE International Conference on Robotics and Automation*, 2017, pp. 5281–5288.

[22] ——, "On the combined inverse-dynamics/passivity-based control of elastic-joint robots," *IEEE Transactions on Robotics*, vol. 34, no. 6, pp. 1461–1471, 2018.

[23] J. Jung, D. Kim, and J. Park, "Operational space control framework for torque controlled humanoid robots with joint elasticity," in *2019 IEEE/RSJ International Conference on Intelligent Robots and Systems*, 2019, pp. 3063–3069.

[24] O. Khatib, "A Unified Approach for Motion and Force Control of Robot Manipulators: The Operational Space Formulation," *IEEE Journal of Robotics and Automation*, vol. RA-3, no. 1, pp. 43–53, February 1987.

[25] L. Sentis and O. Khatib, "Synthesis of Whole-Body Behaviors through Hierarchical Control of Behavioral Primitives," *International Journal of Humanoid Robotics*, vol. 2, no. 4, pp. 505–518, January 2005.

[26] J. Nakanishi, R. Cory, M. Mistry, J. Peters, and S. Schaal, "Operational Space Control: A Theoretical and Empirical Comparison," *International Journal of Robotics Research*, vol. 27, no. 6, pp. 737–757, June 2008.

[27] L. Sentis, J. Park, and O. Khatib, "Compliant Control of Multicontact and Center-of-Mass Behavior in Humanoid Robots," *IEEE Transactions on Robotics*, vol. 26, no. 3, pp. 483–501, June 2010.

[28] A. Dietrich, C. Ott, and J. Park, "The Hierarchical Operational Space Formulation: Stability Analysis for the Regulation Case," *IEEE Robotics and Automation Letters*, vol. 3, no. 2, pp. 1120–1127, April 2018.

[29] L. Righetti, J. Buchli, M. Mistry, and S. Schaal, "Inverse Dynamics Control of Floating-Base Robots with External Constraints: a Unified View," in *Proc. of the 2011 IEEE International Conference on Robotics and Automation*, May 2011, pp. 1085–1090.

[30] K. Bouyarmane and A. Kheddar, "On Weight-Prioritized Multitask Control of Humanoid Robots," *IEEE Transactions on Automatic Control*, vol. 63, no. 6, pp. 1632–1647, June 2018.

[31] K. Otani and K. Bouyarmane, "Adaptive Whole-Body Manipulation in Human-to-Humanoid Multi-Contact Motion Retargeting," in *Proc. of the 17th IEEE-RAS International Conference on Humanoid Robotics*, November 2017, pp. 446–453.

[32] J. Englsberger, A. Dietrich, G. Mesesan, G. Garofalo, C. Ott, and A. Albu-Schäffer, "MPTC - Modular Passive Tracking Controller for stack of tasks based control frameworks," in *Proc. of Robotics: Science and Systems 2020*, July 2020.

[33] A. Dietrich and C. Ott, "Hierarchical Impedance-Based Tracking Control of Kinematically Redundant Robots," *IEEE Transactions on Robotics*, vol. 36, no. 1, pp. 204–221, February 2020.

[34] J. J. Gil, A. Rubio, and J. Savall, "Decreasing the Apparent Inertia of an Impedance Haptic Device by Using Force Feedforward," *IEEE Transactions on Control Systems Technology*, vol. 17, no. 4, pp. 833–838, July 2009.

[35] F. Ghorbel, B. Srinivasan, and M. W. Spong, "On the Uniform Boundedness of the Inertia Matrix of Serial Robot Manipulators," *Journal of Robotic Systems*, vol. 15, no. 1, pp. 17–28, 1998.

[36] H. Sadeghian, L. Villani, M. Keshmiri, and B. Siciliano, "Task-Space Control of Robot Manipulators With Null-Space Com-

pliance," *IEEE Transactions on Robotics*, vol. 30, no. 2, pp. 493–506, April 2014.

[37] J. H. Park, "Impedance Control for Biped Robot Locomotion," *IEEE Transactions on Robotics and Automation*, vol. 17, no. 6, pp. 870–882, December 2001.

[38] A. van der Schaft, *L_2-Gain and Passivity Techniques in Nonlinear Control*, 3rd ed. Springer International Publishing, 2017.

[39] V. Davila Santibáñez and R. Kelly, "Strict Lyapunov functions for control of robot manipulators," *Automatica*, vol. 33, no. 4, pp. 675–682, 1997.

[40] S. P. Buerger and N. Hogan, "Complementary Stability and Loop Shaping for Improved Human-Robot Interaction," *IEEE Transactions on Robotics*, vol. 23, no. 2, pp. 232–244, April 2007.

[41] E. Colgate and N. Hogan, "An analysis of contact instability in terms of passive physical equivalents," in *Proc. of the 1989 IEEE International Conference on Robotics and Automation*, May 1989, pp. 404–409.

[42] S. P. Buerger and N. Hogan, "Relaxing passivity for human-robot interaction," in *Proc. of the 2006 IEEE/RSJ International Conference on Intelligent Robots and Systems*, 2006, pp. 4570–4575.

[43] T. Yoshikawa, "Manipulability of Robotic Mechanisms," *International Journal of Robotics Research*, vol. 4, no. 2, pp. 3–9, June 1985.

[44] J. Englsberger, G. Mesesan, A. Werner, and C. Ott, "Torque-based dynamic walking - A long way from simulation to experiment," in *Proc. of the 2018 IEEE International Conference on Robotics and Automation*, May 2018, pp. 440–447.

[45] R. Bischoff, J. Kurth, G. Schreiber, R. Koeppe, A. Albu-Schäffer, A. Beyer, O. Eiberger, S. Haddadin, A. Stemmer, G. Grunwald, and G. Hirzinger, "The KUKA-DLR Lightweight Robot arm - a new reference platform for robotics research and manufacturing," in *Proc. of the ISR 2010 and ROBOTIK 2010*, June 2010, pp. 741–748.

[46] A. Albu-Schäffer, C. Ott, and G. Hirzinger, "A Unified Passivity-based Control Framework for Position, Torque and Impedance Control of Flexible Joint Robots," *International Journal of Robotics Research*, vol. 27, no. 1, pp. 23–39, January 2007.

[47] S. Haddadin, A. De Luca, and A. Albu-Schäffer, "Robot Collisions: A Survey on Detection, Isolation, and Identification," *IEEE Transactions on Robotics*, vol. 33, no. 6, pp. 1292–1312, December 2017.

[48] C. Gaz, F. Flacco, and A. De Luca, "Identifying the Dynamic Model Used by the KUKA LWR: A Reverse Engineering Approach," in *Proc. of the 2014 IEEE International Conference on Robotics and Automation*, May/June 2014, pp. 1386–1392.

[49] A. De Luca, A. Albu-Schäffer, S. Haddadin, and G. Hirzinger, "Collision Detection and Safe Reaction with the DLR-III Lightweight Manipulator Arm," in *Proc. of the 2006 IEEE/RSJ International Conference on Intelligent Robots and Systems*, October 2006, pp. 1623–1630.

[50] J. Peters, M. Mistry, F. Udwadia, J. Nakanishi, and S. Schaal, "A unifying framework for robot control with redundant DOFs," *Autonomous Robots*, vol. 24, no. 1, pp. 1–12, 2008.

[51] A. Albu-Schäffer, C. Ott, U. Frese, and G. Hirzinger, "Cartesian Impedance Control of Redundant Robots: Recent Results with the DLR-Light-Weight-Arms," in *Proc. of the 2003 IEEE International Conference on Robotics and Automation*, Sept. 2003, pp. 3704–3709.